1. AGENCY USE O... (Leave blank)

.. .. AND DATES COVERED

4. TITLE AND SUBTITLE

HIGH ACCURACY ATTITUDE CONTROL OF A SPACE CRAFT USING FEEDBACK LINERIZATION

5. FUNDING NUMBERS

6. AUTHOR(S)

Louis Joseph Poehlman

7. PERFORMING ORGANIZATION NAME(S) AND ADDRESS(ES)

Northeastern University

8. PERFORMING ORGANIZATION REPORT NUMBER

94-112

9. SPONSORING / MONITORING AGENCY NAME(S) AND ADDRESS(ES)

DEPARTMENT OF THE AIR FORCE
AFIT/CI
2950 P STREET
WRIGHT-PATTERSON AFB OH 45433-7765

10. SPONSORING / MONITORING AGENCY REPORT NUMBER

11. SUPPLEMENTARY NOTES

12a. DISTRIBUTION / AVAILABILITY STATEMENT

Approved for Public Release IAW 190-1
Distribution Unlimited
MICHEAL M. BRICKER, SMSgt, USAF
Cheif Administration

12b. DISTRIBUTION CODE

13. ABSTRACT (Maximum 200 words)

DTIC
SELECTED
AUG 1 2 1994
F
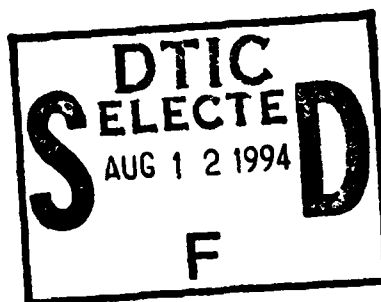
14. SUBJECT TERMS

15. NUMBER OF PAGES

147

16. PRICE CODE

17. SECURITY CLASSIFICATION OF REPORT

18. SECURITY CLASSIFICATION OF THIS PAGE

19. SECURITY CLASSIFICATION OF ABSTRACT

20. LIMITATION OF ABSTRACT

GENERAL INSTRUCTIONS FOR COMPLETING SF 298

The Report Documentation Page (RDP) is used in announcing and cataloging reports. It is important that this information be consistent with the rest of the report, particularly the cover and title page. Instructions for filling in each block of the form follow. It is important to *stay within the lines* to meet *optical scanning requirements*.

Block 1. Agency Use Only *(Leave blank)*.

Block 2. Report Date. Full publication date including day, month, and year, if available (e.g. 1 Jan 88). Must cite at least the year.

Block 3. Type of Report and Dates Covered. State whether report is interim, final, etc. If applicable, enter inclusive report dates (e.g. 10 Jun 87 - 30 Jun 88).

Block 4. Title and Subtitle. A title is taken from the part of the report that provides the most meaningful and complete information. When a report is prepared in more than one volume, repeat the primary title, add volume number, and include subtitle for the specific volume. On classified documents enter the title classification in parentheses.

Block 5. Funding Numbers. To include contract and grant numbers; may include program element number(s), project number(s), task number(s), and work unit number(s). Use the following labels:

C	- Contract	PR	- Project
G	- Grant	TA	- Task
PE	- Program Element	WU	- Work Unit Accession No.

Block 6. Author(s). Name(s) of person(s) responsible for writing the report, performing the research, or credited with the content of the report. If editor or compiler, this should follow the name(s).

Block 7. Performing Organization Name(s) and Address(es). Self-explanatory.

Block 8. Performing Organization Report Number. Enter the unique alphanumeric report number(s) assigned by the organization performing the report.

Block 9. Sponsoring/Monitoring Agency Name(s) and Address(es). Self-explanatory.

Block 10. Sponsoring/Monitoring Agency Report Number. *(If known)*

Block 11. Supplementary Notes. Enter information not included elsewhere such as: Prepared in cooperation with...; Trans. of...; To be published in.... When a report is revised, include a statement whether the new report supersedes or supplements the older report.

Block 12a. Distribution/Availability Statement. Denotes public availability or limitations. Cite any availability to the public. Enter additional limitations or special markings in all capitals (e.g. NOFORN, REL, ITAR).

DOD - See DoDD 5230.24, "Distribution Statements on Technical Documents."
DOE - See authorities.
NASA - See Handbook NHB 2200.2.
NTIS - Leave blank.

Block 12b. Distribution Code.

DOD - Leave blank.
DOE - Enter DOE distribution categories from the Standard Distribution for Unclassified Scientific and Technical Reports.
NASA - Leave blank.
NTIS - Leave blank.

Block 13. Abstract. Include a brief *(Maximum 200 words)* factual summary of the most significant information contained in the report.

Block 14. Subject Terms. Keywords or phrases identifying major subjects in the report.

Block 15. Number of Pages. Enter the total number of pages.

Block 16. Price Code. Enter appropriate price code *(NTIS only)*.

Blocks 17. - 19. Security Classifications. Self-explanatory. Enter U.S. Security Classification in accordance with U.S. Security Regulations (i.e., UNCLASSIFIED). If form contains classified information, stamp classification on the top and bottom of the page.

Block 20. Limitation of Abstract. This block must be completed to assign a limitation to the abstract. Enter either UL (unlimited) or SAR (same as report). An entry in this block is necessary if the abstract is to be limited. If blank, the abstract is assumed to be unlimited.

94-112

CSDL-T-1145

HIGH ACCURACY ATTITUDE CONTROL OF A SPACECRAFT USING FEEDBACK LINEARIZATION

by

Louis Joseph Poehlman

May 1992

Master of Science Thesis
Northeastern University

Accesion For	
NTIS CRA&I	☑
DTIC TAB	☐
Unannounced	☐
Justification	
By	
Distribution /	
Availability Codes	
Dist	Avail and / or Special
A-1	

DRAPER
LABORATORY

NORTHEASTERN UNIVERSITY

Graduate School of Engineering

Thesis Title: High Accuracy Control of a Spacecraft Using Feedback Linearizaton

Author: Louis Joseph Poehlman, Captain, USAF

Department: Electrical and Computer Engineering

Approved for Thesis Requirement of the Master of Science Degree

Howard Musoff   5/27/92
_____
Howard Musoff   Date
Principal Member Technical Staff, The Charles Stark Draper Laboratory
Thesis Supervisor

Clas A. Jacobson   5-28-92
_____
Clas A. Jacobson   Date
Assistant Professor, Department of Electrical and Computer Engineering
Thesis Advisor

Gilead Tadmor   5.28.72
_____
Gilead Tadmor   Date
Assistant Professor, Department of Electrical and Computer Engineering
Thesis Advisor

John G. Proakis   5/28/92
_____
John G. Proakis   Date
Chairman, Department of Electrical and Computer Engineering

Graduate School Notified of Acceptance:

Freeman   5/29/92
_____
Director, Graduate School   Date

High Accuracy Attitude Control of a Spacecraft Using Feedback Linearization

A Thesis Presented

by

Louis Joseph Poehlman, Captain, USAF

B.S., U.S. Air Force Academy (1983)

to

The Department of Electrical and Computer Engineering

in partial fulfillment of the requirements
for the degree of

Master of Science

in the field of

Electrical Engineering

Northeastern University
Boston, Massachusetts

May 28, 1992

High Accuracy Attitude Control of a Spacecraft Using Feedback Linearization

by

Louis Joseph Poehlman, Captain, USAF

Submitted to the Department of Electrical and Computer Engineering
on May 28, 1992, in partial fulfillment of the
requirements for the degree of
Master of Science

Abstract

The initial architecture and controller design for a small satellite is proposed, using a two degree of freedom gyroscope on a two axis stabilized platform for pointing and estimating the spacecraft body angular rates, with a second gyro mounted on the spacecraft which measures the third spacecraft body rate component. The spacecraft configuration includes a three axis reaction wheel assembly and a large aperture optic fixed to the spacecraft which must be commanded to acquire an Earth-fixed target. The stable platform and optical payload have the same line of sight, and the approach developed was to command the platform as a free body to line its unit target vector line of sight with its line of sight; the spacecraft then is commanded to follow the platform and maintain the angular displacement between the platform and spacecraft near null. The platform controller is designed using nonlinear feedback to linearize and decouple the input/output mapping using the target unit vector direction cosine components as the controlled variables which are controlled in a linear manner by use of a fixed-time optimal controller. The spacecraft then follows the platform rate commands by commanding the reaction wheel assembly based on the commanded rates to the stable platform and a platform motion compensation feedforward command which regulates the angular displacement between the platform and spacecraft. The computed torque to the reaction wheels is accomplished by a nonlinear controller which linearizes and decouples the basic rigid body equations of motion where the controlled variables are the angular rates of the spacecraft. The performance improvements of the nonlinear controllers over linear controllers are verified by simulation of the spacecraft nonlinear system model for cases involving large angle reorientations and using both ideal and uncertainty models for the spacecraft inertia tensor and angular rates.

2

Acknowledgements

I extend my sincerest gratitude to my thesis supervisor at the Charles Stark Draper Laboratory, Dr. Howard Musoff. He was constantly supportive of my efforts and provided me with a deep appreciation for those who can bridge the gap between applied mathematics and engineering problem solving. He is a true mentor and friend, and this thesis reflects on his constant and sure guidance of my research.

I also thank my Northeastern University thesis advisors, Professor Clas Jacobson and Professor Gilead Tadmor, for introducing me to the concepts of active learning and mathematical reasoning. In particular, Professor Jacobson took a keen interest in my education and helped me break through critical problems throughout my thesis research. He instilled in me an appreciation for structure in thinking and problem solving, and I will never forget to apply the "What does it mean, and why do I care?" philosophy to my continuing education and future career activities. He also introduced me to typesetting using LaTeX, which made preparation of the thesis manuscript possible.

I have the great fortune of a wonderful family which has influence me in many ways. My wife Athena provided me with much needed perspective and was a reservoir of emotional strength for me throughout my pursuit of this degree. My father's Air Force career and engineering background was a major influence on my own career choices and I am grateful for his loyalty and guidance. My grandfather affected me in a profound way, by providing a work-ethic role model which carries me forward from my childhood, and this thesis is dedicated to his memory.

I also would like to thank all of my friends and associates throughout my career who have challenged, entertained, and stimulated my interests in the space sciences. I have had the privilege of learning space systems and the operational perspective from many of the pioneers in the field and a dedicated and professional group of individuals whose goal has always been to complete the mission. I hope their wisdom and experience has shaped this thesis to make it a potentially useful contribution towards future space operations.

Finally, I would like to thank the U.S. Air Force and the Charles Stark Draper Laboratory for giving me the opportunity to pursue an advanced degree in the best possible learning environment. This thesis was prepared at The Charles Stark Draper Laboratory, Inc., under Company Sponsored Research funding. Publication of this report does not constitute approval by the Draper Laboratory, the U.S. Air Force, or Northeastern University of the findings or conclusions contained herein. It is published solely for the exchange and stimulation of ideas.

I hereby assign my copyright of this thesis to The Charles Stark Draper Laboratory, Inc., of Cambridge, Massachusetts.

Louis J. Poehlman

Permission is hereby granted to The Charles Stark Draper Laboratory, Inc. and to Northeastern University to reproduce and to distribute copies of this thesis document in whole or in part.

3

Contents

List of Figures

8

List of Tables

Chapter 1

Introduction

The design of an Earth-orbiting satellite encompasses many engineering disciplines whose goal is to maximize the mission capability of a spacecraft while constrained by size, mass, orbital parameters, on-board computing power, manufacturing technology and cost. While large spacecraft such as the Hubble telescope or space station *Freedom* embody pushing the envelope of capability at the high end of the booster and cost spectrum, the working advantages of remote sensing and communications may be met in the future by small, short lead time, cost-effective constellations of satellites. Commercial boosters such as the Orbital Sciences *Pegasus* point the way to this arena. The Charles Stark Draper Laboratory (CSDL) is researching the use of advanced navigation, guidance and control techniques to produce an autonomous spacecraft control system suitable for such applications. In particular, this thesis takes advantage of a capability currently under development at CSDL, namely the Inertial Pseudo Star Reference Unit (IPSRU), which is a stable platform used to provide high bandwidth image stabilization through the use of a collimated light source injected into the optic. This reference can be used in a closed-loop fashion to control image smear by commanding a fast steering mirror to cancel the error signal from the pseudo-star reference beam. This platform uses an extremely high accuracy two axis gyroscope which is used to not only control the inertially stabilized platform, but will be used to provide an attitude data reference, as developed in this thesis.

This thesis is essentially a snapshot of a portion of the overall spacecraft design process for a small satellite with a remote sensing application which uses a the IPSRU stable platform for both image stabilization and attitude determination and control to point the optical payload. The

elements and tradeoffs of this process are included to highlight the issues which need continual attention as the overall system is developed. Mission planning and operational considerations are illustrated but are not sufficiently detailed other than to provide insight into the attitude determination and control subsystem architecture. The approach throughout the thesis is deterministic and relies heavily on classical rigid body kinematics and dynamics. The controller designs include aspects of both linear and nonlinear control theory, and the reader should at least be familiar with the optimal control methods detailed in texts such as references [6] and [15]. A detailed literature search was conducted regarding the attitude control of satellites using momentum exchange devices, and though basic techniques were adapted from recent references on the use of exact linearization (such as [8] and [27]), the specific control approach developed in this thesis appears to be unique. The intended audience for the design presented here includes theorists who are interested in examining a design study and practicing engineers who may find the design applicable to their problem, specifically those who will continue this research effort as other subsystems of the design are developed and the architecture presented here is refined. The results include the architecture, the actual controller design and the controller simulation which is described in detail.

1.1 Problem Statement

The problem is to design the attitude control architecture for an autonomously controlled, small, low earth orbiting spacecraft whose primary mission it to point a payload optic at an Earth-fixed target. No specific payload is identified so preliminary mission planning rules of thumb are used to determine the fundamental physical requirements for both performance and actuator sizing. The spacecraft configuration was developed as part of a study at CSDL [26]. The spacecraft is sized to fit into an Orbital Sciences *Pegasus* launch booster, which limits its dimensions, mass and orbit. High accuracy requirements assumed for an optical payload which is a part of the spacecraft structure necessitates the use of 3-axis stabilization through the use of some form of momentum exchange devices; in this case a reaction wheel assembly (RWA) is used which must be sized for absorption of disturbances and slewing requirements. The spacecraft is autonomous and must be capable of pointing at a target vector which is uploaded to the spacecraft, so the control system must be capable of determining its attitude

on-board the spacecraft and computing the commands to control the attitude to point the optic at the target with precision. The desire for a low-cost approach leads to the use of an existing inertially stabilized platform's two degree of freedom (TDOF) dynamically-tuned gyro (DTG) as the primary attitude reference for the platform with an additional gyro mounted on the spacecraft for the third axis. The gyro data is supplemented by filtering of other sensors required for the initial deployment (e.g. earth and sun sensors) and/or star acquisition data from the optic; this filter is another on-going study at CSDL [20]. The thesis is based on the assumption the gyroscope data is calibrated. The angular displacement between the IPSRU platform and the spacecraft is physically limited and must be kept near null to allow the stable platform to operate successfully.

Design Goals

Performance specifications are hard to determine without a defined mission for the spacecraft, but the general mission outlined here requires a high-accuracy capability. In the context of typical satellites of this type this means a pointing requirement of less than 0.01 degrees error [30]. A potentially significant portion of the error source for Earth target acquisition is the knowledge of the orbit; thus it is assumed the orbit is determined externally to the attitude control system using either the Navstar Global Positioning System (GPS) or some other method of generating an accurate ephemeris. Thus the control system can be analyzed based on expected disturbances, process uncertainty, and measurement uncertainty assuming perfect knowledge of the orbital position. This thesis is the first design attempt for this spacecraft's attitude control system so the major goal is to validate the approach used and highlight the significant design issues which must resolved as the design progresses through the next iteration. The goal of autonomous navigation and control makes this objective even more important. Therefore, the general goal simply stated is to validate the design spacecraft control laws which show promise of acceptable performance under the influence of known disturbance magnitudes and generic system uncertainty. With the mission in mind, several distinct objectives can be formulated:

1. Determine the control law for the inertially stable platform which will generate gyro rate commands to the platform causing it to point at a target (assumed to be, but not limited to, an Earth-fixed target).

2. Design a controller which will determine torque inputs to the RWA which will follow the IPSRU rate command and keep the angular displacement between IPSRU and the space-craft less than 10 mrad while not exceeding the bandwidth of the RWA (approximately 0.5 Hz).

3. Minimize effects of known disturbance torques.

4. Compare and contrast linear and nonlinear controllers for performance under ideal con-ditions and conditions where plant and measurement uncertainty are considered.

5. Validate the approach of using the IPSRU gyros to estimate the spacecraft rates and control the line of sight pointing.

Figure 1-1: Inertial Pseudo Star Reference Unit Application

Inertial Pseudo-Star Reference Unit Description

This description is included because a major portion of the satellite design and controller architecture was developed in order to take advantages of the capabilities of the IPSRU payload. The thesis is concerned with the fact that an extremely accurate two axis gyroscope (the DTG) is on the platform, which can provide attitude information for the spacecraft body. The design intent of the IPSRU payload also fits in with the overall concept of the small spacecraft architecture as the goal of the payload is to reduce image smear to due jitter of the optic at high frequencies. Figure 1-1 illustrates the concept. A collimated light source with a high signal-to-noise ratio is injected into the optic from the stable platform and follows the optical path all the way to a beam splitter which diverts the pseudo-star reference beam to a quad cell detector. Any jitter between the inertially stable platform and the optic may be sensed by the detector and a fast steering mirror can be controlled to compensate for the effect and reduce image smear. There are several advantages in using the IPSRU platform for an optical payload:

1. A smaller optic can be used with improved resolution, or a larger optic may take advantage of the increased capability (subject to physical limits of the imaging wavelength.)

2. The optic is mounted to a base, such as a spacecraft structure, and can therefore be larger to take advantage of the spacecraft structure compared to a conventionally controlled aperture.

3. The burden of precision manufacturing is placed on the IPSRU platform, especially in terms of aligning the gyroscope output axes to an arbitrary reference frame.

4. The pseudo star may be used on multiple payloads on the same spacecraft bus, thus saving cost, weight, power and complexity of the payloads and the spacecraft bus.

The term "IPSRU" is used extensively throughout the thesis in order to maintain consistency with ongoing engineering efforts regarding its applications. For purposes of the thesis it is a stable platform whose two-axis gyro is used to estimate the spacecraft body attitude and whose reference beam line-of-sight (LOS) must be pointed at the desired target to ensure the target is in the optic field of view (FOV). A second gyro of the same type is mounted at the base of IPSRU to provide attitude information for the third axis.

14

Attitude Control Concept

Attitude control of a rigid body rotating in space presents an interesting control problem for exploring the concepts of both nonlinear (in this case feedback linearization) and optimal control as the system physics are straightforward and there is a great deal of practical experience in such applications. In fact, much of this thesis is spent on specific details of developing the kinematics and dynamics for the particular application of pointing using the stable platform as the reference for the spacecraft attitude. The conceptual framework for the attitude control approach is illustrated in Figure 1-2. For small angle slews and perturbations around an arbitrary vehicle orientation, the typical model for a spacecraft is simply a double-integrator around each decoupled principal axis as described in [14] and [30]. However, if the nonlinearities and cross-coupling are not ignored, it is possible to determine a nonlinear transformation which puts it into the desired form. The attitude of the IPSRU platform is parameterized by a direction cosine matrix (DCM) which can be computed by integrating the commanded inputs to the stable platform gyro and by making use of the angular displacement measurement between the platform and the base plus the third axis gyro measurement. The spacecraft attitude can be estimated by using the same approach: transform the attitude by use of the angular displacement sensors between the platform and the spacecraft. The spacecraft can then be commanded to follow the commanded rates to the stable platform to keep the angular displacement near null. Details of this process are developed in Chapter 3 and the appendices.

Literature Search Results

The literature search focused on attitude control of a spacecraft using momentum exchange devices. The search was conducted on English language references from 1965 to the present, resulting in a very large list of abstracts. A narrower search for the period 1982 to the present resulted in over 500 references whose abstracts were reviewed resulting in the review of over 60 references. The concept of the feedback linearization of the unit quaternion from several of the references appeared to show promise for the application, so the thesis was formulated to attempt a comparison of this technique with linear control techniques such as those found in [13] or [14]. The search was by no means exhaustive, and the attitude control problem is still an area of active research as evidenced by the recent article *The Attitude Control Problem* [29].
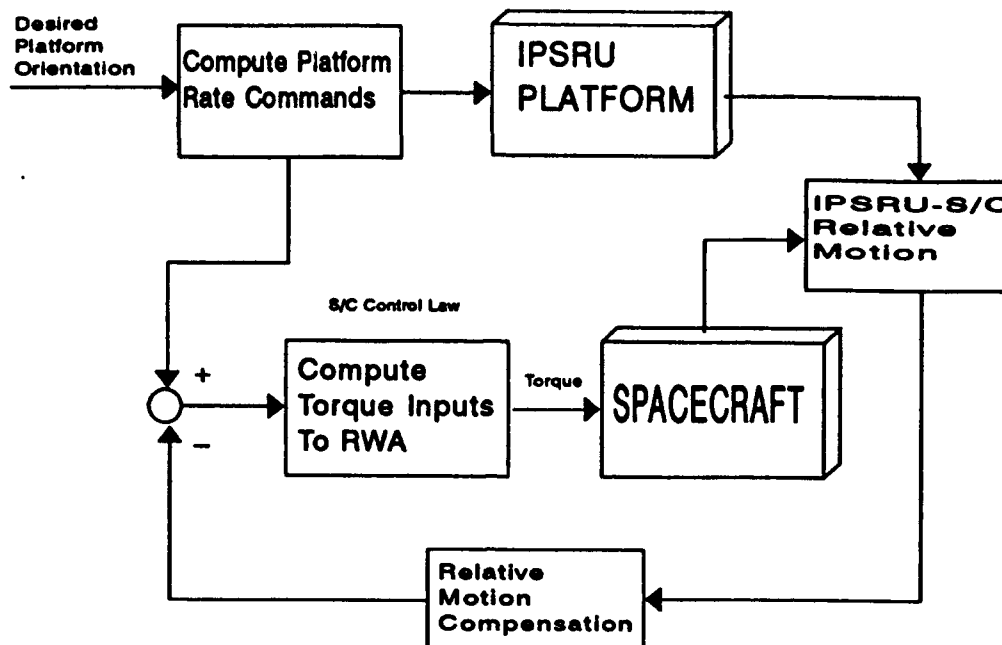
Figure 1-2: Attitude Control Concept

The concept of canceling nonlinear dynamics by dynamic controllers goes back as far as Truxal [28] and has been a fundamental formulation in robotics and adaptive control [2]. The following references are a limited sampling of sources for additional information on these topics:

Linear Optimal Control Theory References [4], [6], [9], [15], [16] and [18].

Nonlinear Control Theory (Feedback Linearization) References [12] and [27].

Spacecraft Attitude Control References [1], [8], [11], [13], [14], [31], [23],[29] and [30].

1.2   Summary of Key Findings

The overall results of the thesis are successful. Simulations indicate the architecture works for both linear and nonlinear controllers, with a performance advantage in controlling the

16

desired angular rates by the use of nonlinear controllers based on feedback linearization. Other interesting results are noted:

1. Demonstration that the use of feedback linearization results in lower peak wheel speeds and smaller angular displacement between the platform and the spacecraft, in particular for one-axis slews and compared with a linear controller where there is uncertainty in the inertia tensor.

2. The use of the IPSRU gyro input commands in estimating the spacecraft rates appears to be feasible, with errors accumulating due to persistent biases indicating a requirement to recalibrate the gyros periodically (or to filter them with other attitude measurements).

3. Target pointing based on two elements of a direction cosine matrix under one constraint, resulting in two scalar equations which is simpler than recent references which use the four elements of the unit quaternion [8] [29]. This is accomplished by a restriction of spacecraft slew angles to less than 90 degrees, which is acceptable for the suggested mission.

4. The use of a linear finite-time optimal control approach to controlling the IPSRU platform to align with a unit target vector.

5. Illustration of a complete attitude control design process with related issues highlighted for future study.

These and other findings are summarized at the end of Chapters 4 and 5 and in Chapter 6.

1.3   Thesis Outline

The thesis is organized as follows:

Chapter 1 is the introduction and motivation for the thesis.

Chapter 2 provides the basic spacecraft configuration and mission planning impacts on the control design approach.

Chapter 3 develops the controller architecture and design.

Chapter 4 describes the controller design process and platform control simulation results.

Chapter 5 describes the simulation results for the overall spacecraft under both the ideal model and a model using a perturbed plant and measurement noise.

Chapter 6 summarizes the results and lists many of the issues raised by this initial design. Recommendations for future reasearch and design are also presented.

Appendix A describes the notation used throughout the thesis.

Appendix B describes the coordinate frames of interest and why they were chosen.

Appendix C derives a method for determining the target motion in the IPSRU frame from an autonomous spacecraft approach.

Appendix D derives the platform kinematic relationships used in attitude estimation and control of the platform angular displacement.

Appendix E describes the simulation technique.

Chapter 2

Mission Overview and System Description

The control system for a spacecraft is significantly intertwined with the evolution of the space-craft mission and hardware configuration. The purpose of this chapter is to outline the baseline mission and spacecraft configuration used for the control system design developed in this thesis. The basis for discussion of both the orbital analysis and the spacecraft control design are very dependent on the coordinate frames of reference, which are described first. The orbit itself is based on several factors and is included to give a realistic baseline for both the spacecraft configuration and control system sizing. The orbit and the hardware configuration then provide a basis for describing the disturbance environment which in turn forms allows determination of some performance goals. This process is iterative and the control design for this thesis uses a baseline "snapshot" of the initial design for a spacecraft.

The mission of this spacecraft has not been specifically determined, other than it is assumed to be some type of large optical payload with both surveying and targeting modes. In a surveillance mode the spacecraft is pointed towards nadir (the center of the Earth's geopotential) and the orbit trace itself provides the data path, and anything within the optical field of view is potentially visible. In targeting mode the spacecraft points at a particular ground fixed target as it passes nearby, and therefore the spacecraft must be able to get the target within the field of view of the optic and keep it there to provide quality data. An example of surveillance

19

might be a payload which looks for volcanic eruptions as it circumvents the globe, perhaps locating them as well. A targeting mode for this example would be to look at, for example, a specific location in the Amazon forest as the spacecraft passes nearly overhead. Both examples require the target element to be pointed at a known location accurately, which implies accurate knowledge of the spacecraft's attitude.

2.1 Coordinate Frame Descriptions

There are several coordinate frames used in this analysis which were chosen to provide advantages in analysis of the orbit, platform kinematics and spacecraft dynamics. The coordinate frame descriptions are not sufficient for analysis purposes; a thorough understanding of their relationships, via coordinate transformations, is also essential for both computational and intuitive reasons. Appendix A gives a more thorough description of the general descriptions provided in this section.

Earth-Centered Inertial Frame

The Earth-Centered Inertial (ECI) frame is essentially described by a plane through the Earth's equator, with the z-axis pointed towards the North Pole. The x-axis points towards the "first point of Aries," or the direction of the position where the ecliptic plane intersects the equatorial plane as the sun travels South to North. The y-axis is then orthogonal to the x - axis and z - axis. It is considered sufficiently inertial for most satellite applications, and is typically used for satellite orbital descriptions and Earth-based inertial navigation.

Earth-Centered Earth-Fixed Frame

The Earth-Centered Earth-Fixed (ECF) frame uses the same fundamental plane as the ECI frame, only the x axis is fixed to the earth. For this study the position of the x-axis is assumed to be whatever position the GPS receiver uses as a reference, typically WGS-84 coordinates [5].

Inertial Frame

The inertial frame is the absolute reference for all kinematics and dynamics, and is arbitrary as long as it is inertial. The inertial frame for this study is determined by comparisons of star catalogs with fixed star sightings, and is updated at each gyro stellar calibration. It is used here as the starting point for all inertial references (e.g. gyroscopic outputs).

Spacecraft Body-Fixed Frame

The spacecraft body-fixed frame (B) is fixed to the spacecraft rigidly and is assumed to be through the center of mass and along the directions of the principal axes. Note this assumes that the principal axes are aligned with the geometric axes and that the reaction wheel output axes are aligned with the frame. The first assumption is tested in this thesis.

IPSRU-Fixed Frame

The fundamental plane of this frame is assumed to be formed by the output axes of the two degree of freedom dynamically tuned gyro (DTG). The z-axis is orthogonal to the output axes and is assumed to be along the direction of the pseudo-star reference beam line of sight. IPSRU is treated as a free rigid body for the kinematic equations of motion and is connected to the spacecraft as a rigid body attached via a flexure hinge about two axes. This frame is used for two reasons: the inertial reference outputs from the IPSRU DTG are conveniently described in this frame and the desire to control the IPSRU reference beam line-of-sight (LOS) which is essentially the same as pointing the IPSRU-fixed frame z-axis towards the desired target.

Coordinate Frame Summary

Table 2.1 summarizes the key features of the coordinate frames.

2.2   Orbital Parameters

This section is included to describe the type analysis required prior to final control system selection and design. The orbit directly influences the nature and magnitude of attitude perturbations due to the earth's influence on the satellite in orbit. For a pointing application,

Table 2.1: Coordinate Frame Characteristics

FRAME	SUBSCRIPT	TYPE	ORIGIN	FUNDAMENTAL PLANE	X-AXIS
Earth-Centered Earth-Fixed (ECF)	E	Rotating	Earth Center	Equatorial Plane Orthogonal to Mean Polar Axis	0.544" East of Greenwich Meridian
Earth-Centered Inertial (ECI)	C	Inertial	"	"	Vernal Equinox Direction
Inertial	I	Inertial	IPSRU Center	Fixed by Two Star Sightings	Along First Sighting
IPSRU	P	Rotating	"	Orthogonal To IPSRU Reference Beam	Aligned With DTG x-Axis
Spacecraft Body-Fixed	B	Rotating	S/C Center	Orthogonal To S/C z-axis Gyro	Aligned With S/C x-axis RW

it also determines the maximum field of view and related slewing requirements. In fact, the orbit directly and indirectly affects all aspects of the spacecraft's design, which are intertwined significantly. Therefore, there is no optimum design which can account for all factors involved, but experience has led to various methods of sizing proven designs and/or iterative methods based on budgeting related requirements between subsystems. For the desired low orbiting lightweight satellite, several orbit options are available but historically the minimum altitude is around 90 km and the maximum is around 700 km [31]. A complete Earth coverage requirement for an optical payload requires either a constellation or some type of polar orbit.

From a practical standpoint, however, the mission ultimately describes the particular orbit, but other factors such as cost, spacecraft and payload size (resolution), booster availability and capability, constellation size, and desired spacecraft lifetime are all taken into account as tradeoffs are made. Cost is not addressed here other than to articulate the desire to design a "low-cost" satellite that has significant capability. The spacecraft is sized to fit a small booster in order to meet the cost requirement, which places severe restrictions on the payload capability in terms of both the spacecraft configuration and the possible orbits which are achievable for a given booster for a given spacecraft mass. A "constellation" of satellites consists of several satellites designed to provide Earth coverage for various requirements, including ground

visibility and fault tolerance requirements; the constellation of Global Positioning Satellites (GPS) is a good example. Although the satellite described here is not designated for a particular constellation or mission, its generic mission is sufficient to determine key orbital parameters which affect both the disturbance environment and mission pointing requirements.

The most critical factor in this study was the intent to use an Orbital Sciences *Pegasus* launcher [26]. This severely restricts the size of the payload and also constrains the maximum achievable altitude for a given spacecraft mass. These both affect the sizing of the other spacecraft subsystems, most notably the power and structural subsystems as solar panels were determined to be needed to provide enough power for a reasonable suite of payload and subsystem parameters [26].

Other factors considered included the resolution requirements of the optic, Earth coverage under various modes of operation, and sun angle constraints on the solar panels. After some iteration, the final orbital parameters were a sun-synchronous orbit of 555 km [26]. The sun synchronicity guarantees the orbital plane will precess at the same rate as the Earth's motion around the sun, which has the desirable effect of allowing a consistent angle of incidence of the sun's rays on the spacecraft (assuming the spacecraft holds a nadir pointing attitude). This allows for some reduction in the complexity of the control of the solar panels and also reduces the complexity of some of the mission planning. The required inclination of the orbit plane for this orbit is 98 degrees, which is nearly polar and also provides near-total Earth coverage.

The field-of-view (FOV) from a particular point of the orbit is approximated by the use of spherical geometry. The first concern for the field of view is the actual area which is potentially visible at a particular instant of time from the orbit. The following assumptions are made primarily because this analysis is included to provide rough bounds on performance requirements for payload which has not been defined.

1. The Earth is circular. In fact, the Earth is roughly an oblate spheroid. The mean radius of the Earth is used, 6378.14 km [30].

2. The FOV is for the spectrum of visible light.

3. The FOV is designated for the side-to-side view of the Earth as viewed from the flight path of the satellite.
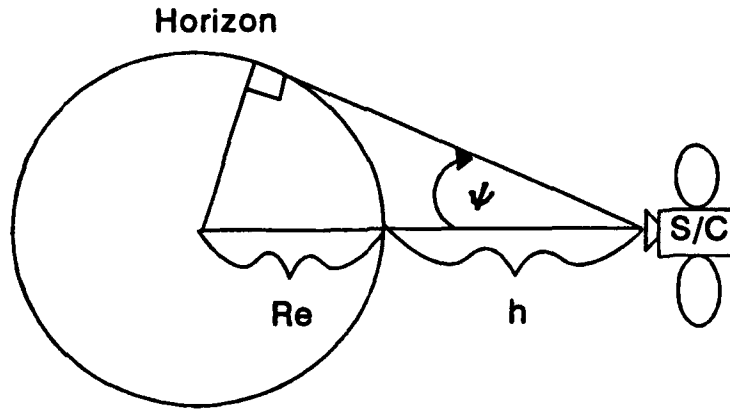
Figure 2-1: Horizon Field of View Geometry

Figure 2.2 illustrates the geometry for the apparent size of the Earth as viewed from the spacecraft, where the following variables are defined:

R_E Radius of the Earth.

h Altitude of the spacecraft above the Earth.

ψ FOV half-angle (radius).

Thus the field of view can be determined:

$$ FOV = 2\psi = 2\left(\sin^{-1}\left(\frac{R_E}{R_E + h}\right)\right) \tag{2.1} $$

Using this approximation the field of view for an altitude of 555 km is approximately 134 degrees. However, the satellite does not have to be able to slew this full range for two reasons. First, the true geometric horizon is not usable due to foreshortening effects; a rough approximation is 30% of the horizon is not usable [31]. Second, the payload optic has a field of view and the goal is not to center the payload in the field of view but to acquire it in the field of view. The optic is assumed to have a field of view of 10 degrees. Thus for a horizon-to-horizion slew the spacecraft will have to be able to slew approximately 70 degrees. Figure 2-2 illustrates a

typical one orbit revolution ground trace for such a swath. As the ground trace continues rev by rev, eventually nearly all of the Earth's landmass is covered even for a simple nadir pointing mission. The large slew would not normally be required or advisable from a mission planning perspective, yet the capability provides significant flexibility for high priority missions.
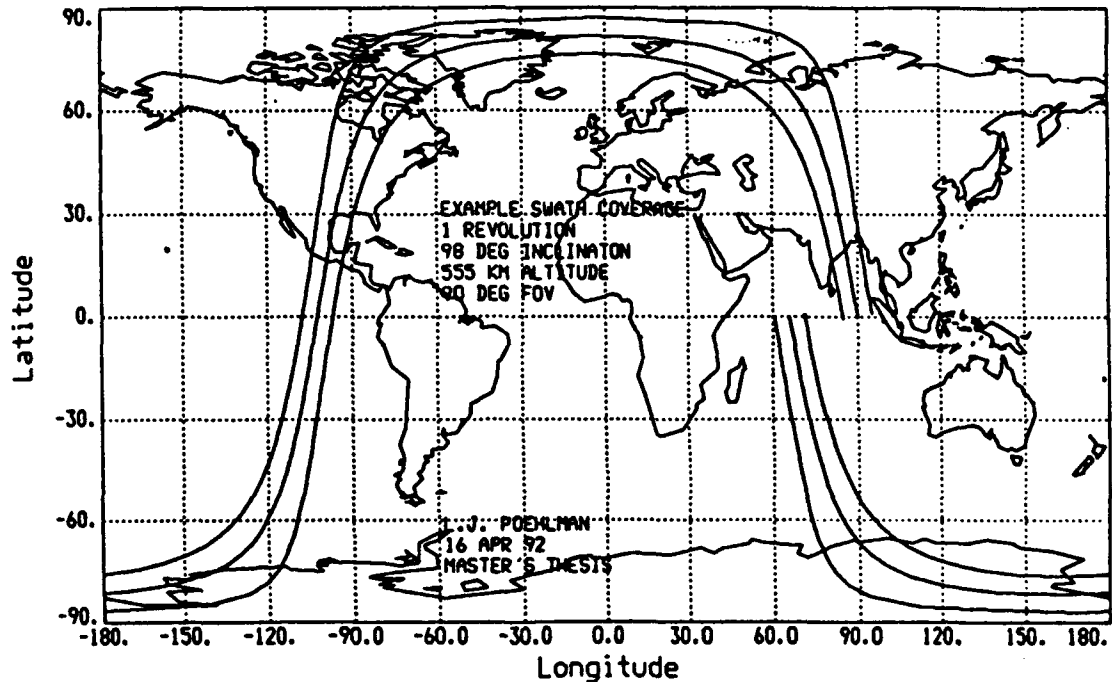
Figure 2-2: Typical Satellite Swath Ground Trace

2.3 Disturbance Environment

The orbital environment is relatively benign from a disturbance standpoint, and disturbances have been characterized based on analysis of spacecraft in orbit over the last twenty-five years. The goal of this section is to determine bounds on the more significant disturbances. Disturbances in this context are external torques acting on the spacecraft. In the absence of these torques, angular momentum is totally conserved (except for internal energy dissipation) and the reaction wheels could be commanded to avoid building up excessive wheel speeds. In reality,

25

the reaction wheels absorb the external torques and as a result the reaction wheels will build up angular momentum which require some form of momentum unloading, such as gas jets or magnetic torquers. Thus the reaction wheels are sized to allow for both the required slewing rates and some extra margin in the wheel speeds to account for this buildup of momentum. The analysis used here follow "rules of thumb" for spacecraft design from [1], [11], [31] and [30]. One additional complication for this analysis was the slewing of the spacecraft; typically spacecraft are oriented towards nadir while the payload is articulated, which means the cyclic torques due to the Earth's geopotential variations can be accurately simulated, and fall mostly on the "pitch" axis of the spacecraft. The expected slewing of this spacecraft invalidates that approach, so all three axes are sized for the worst case which will never happen simultaneously in all three axes.

The orbit of the satellite is a major factor on the effects of various potential sources of external torques to the attitude. For example, a geosynchronous satellite may experience solar wind torques as a dominant torque, while low Earth satellites may find drag in the particles of the upper Earth atmosphere contribute to attitute torques. The torques which were determined to be significant for the projected orbit of this spacecraft (low Earth orbit) are gravity-gradient, aerodynamic, solar pressure and magnetic torques.

2.3.1 Gravitational Effects

Although the spacecraft is small relative to the Earth and for orbit determination and analysis purposes is considered a point mass, in fact it is a somewhat amorphous body with mass properties which vary as a function of the spacecraft attitude and the actual gravity forces acting on each particle. The Earth itself is not a uniform sphere and as a result one portion of the spacecraft may have a different gravity potential acting on it than another. Finally, the orientation of the spacecraft may result in one end of the spacecraft being closer to the Earth, thus having more gravitational potential acting on it than another. The following assumptions are made to determine the magnitude of the gravitational torque:

1. Only Earth gravity is considered (no third body effects.)

2. Spherical Earth.

3. Spacecraft mass $\ll$ mass of the Earth.

4. Spacecraft is a rigid body in a circular orbit.

The gravity gradient torque under these assumptions is derived from the general differential equation for torque due to force acting on a rigid body, integrated over the volume of the spacecraft [11]:

$$\underline{T}_{GG} = \frac{3\mu}{R^3} [\underline{R} \times (J\underline{R})] \tag{2.2}$$

where

J Inertia tensor of the spacecraft.

μ Gravitational constant for the Earth.

R Radius of the satellite orbit.

A first approximation to this effect can be modeled by considering the maximum excursion of some angle γ around the axis of smallest inertia, with the maximum torque exerted on the axis of largest inertia. The maximum torque is then approximated by [11]

$$T_{GG} = \frac{3\mu}{R^3} |J_{max} - J_{min}| \gamma \tag{2.3}$$

When the spacecraft parameters are used in Equation 2.3, and assuming the maximum excursion is $\pi/2$ radians from nadir, the maximum expected persistent gravity gradient torque exerted on the spacecraft is 3.3×10^{-4} N $\cdot$ m.

2.3.2 Aerodynamic Effects

Low orbiting spacecraft may fly within the envelope of particles surrounding the Earth (at or above the upper reaches of the atmosphere) which collide with the leading edge of the spacecraft, creating drag. This effect varies with the orbit, the coefficient of drag for the spacecraft (which varies with orientation relative to the velocity vector), and variations in the atmosphere due to thermal expansion/contraction, solar flares, etc. For a conservative estimate the spacecraft is

assumed to have a coefficient of drag (C_d) of 2.2, as suggested in [11], [31] and [30]. Assuming a circular orbit with constant atmospheric density, the cross section of the spacecraft going along the velocity vector is assumed to be constant and the resulting force can be approximated by [31]:

$$F_{aero} = -\frac{1}{2}p \ A \ C_d \ v^2 \qquad (2.4)$$

where

A is the effective surf᛬ area of the vehicle (1 m).

p is the atmospheric density at the spacecraft altitude (kg/m^3).

C_d is the coefficient of drag ("ballistic coefficient") of the vehicle.

v is the velocity of the vehicle (m/sec).

The torque acting on the vehicle as a result of this force depends on the moment arm, which is the offset of the center of mass from the direction of the force. As this is highly dependent on the spacecraft attitude, a worst-case attitude is assumed where the maximum surface area is exposed at the edge with the longest moment arm. Additonally, the worst case atmospheric density is determined from the atmospheric model used; in this case the worst-case density for 500 km orbit was determined from Larson [31] to be 3.1×10^{-12} kg/m^3. The maximum moment arm length is determined from the spacecraft size and is 0.5 meters. The velocity of the satellite in a polar circular orbit at 550 km is 7.572 km/s [26], and the subsequent torque can be computed by assuming the force acts on the maximum moment arm, resulting in a maximum expected torque of 1.955×10^{-4} N $\cdot$ m $\cdot$ s. Of course, the spacecraft may be changing attitude and the atmospheric density will vary throughout the orbit, but this number gives a rough idea of the maximum magnitude of disturbance torque due to aerodynamic effects.

2.3.3 Solar Pressure Effects

Solar pressure acts in a very similar manner to the aerodynamic effects, in that energy is added to the spacecraft via collisions with solar wind particles. Sources of the disturbance include

solar pressure due directly to the Sun ("solar wind"), the albedo of the Earth, and other less significant sources of energy. The effect is modeled similarly to that of aerodynamic effects, except that the particles do not act uniformly in elastic or inelastic collisions. For example, the solar panels are assumed to absorb the energy while the spacecraft may be reflective. To simplify matters a composite body is modeled with a reflectance factor of 0.6. The angle of incidence relative to the sun then determines the effect of the solar pressure on the spacecraft based on the geometry of the vehicle. The vehicle is modeled as a plane surface since the spacecraft will maintain the solar panels oriented towards the sun (by design and the advantages of the sun-synchronous orbit). The solar radiation torque can then be approximated by [31]:

$$T_{SP} = P \ A \ l [1 + q] \cos(\delta) \tag{2.5}$$

where

P is the solar constant ($4.617 \times 10^{-6} \text{N} \cdot \text{m}$).

A is the surface area of the vehicle exposed to the radiation, 7.35 m.

l is the offset of the center of mass from the center of pressure, which is in effect the "moment arm" acting to create the torque.

q is the composite (essentially specular) reflectance factor (0.6).

δ is the angle of incidence of the solar radiation.

Using this approximation the maximum solar torque is 8.1×10^{-6} N $\cdot$ m.

2.3.4 Magnetic Torques

The Earth's magnetic field is variable and not well characterized, yet its general shape and intensity has been empirically determined. The spacecraft is not composed of totally non-permeable components, and therefore is influenced by the Earth's magnetic field. For a small satellite the effects will be negligible as the dipole moment for the satellite will be very small; by artificially increasing the dipole moment with magnetic coils an additional torque can be produced for the advantageous purpose of desaturating reaction wheels by inducing an applied

"external" torque opposite the desired cross-coupled momentum vector which will cause the reaction wheels to spin down as they react to the torque. This method is slow and inaccurate for attitude control alone because of the large variations in the Earth's magnetic field which are difficult to predict, although the general shape of the Earth's dipole moment is fairly well known [30]. For the polar orbit and altitude of 550 km, the dipole of the Earth B is approximately 0.525 gauss, and the resulting torque acting on the spacecraft is approximated [26]:

$$T_{MAG} = D\ B \times 10^{-7} \tag{2.6}$$

where D is the residual dipole of the vehicle (1000 pole · cm). The result is an estimated worst case magnetic disturbance torque of 5.25×10^{-5} N · m.

2.4   Spacecraft And Attitude Control System Configuration

The initial spacecraft configuration for this study was developed by Pepin [26] and is summarized here. The approach used was to use a combination of scaling existing designs where possible and rough tradeoffs for those items which could not be scaled. A weight and power budget for the various subsystems was developed under the launch vehicle throw weight constraint and payload faring sizing constraint. Additional tradeoffs were then made based on telescope sizing versus resolution at various altitudes and orbital inclinations. Although all the parameters of the configuration are interrelated, the structure, payload, and attitude determination and control subsystems are of real interest to the control law design and analysis.

2.4.1   Spacecraft Configuration

The satellite is basically cylindrical in order to maximize the use of space in the payload faring. The power needed for the satellite cannot be met by solar cells affixed to the body of the spacecraft, thus solar panels are required. Solar panels are deployed after orbital insertion, resulting in a "cylinder with wings" configuration as shown in Figure 2-3. The payload optic points toward the Earth in the nominal nadir pointing mode with the solar panels oriented orthogonal to the sun line. Reaction wheels maintain the spacecraft orientation, and are mounted along the principal axes of the spacecraft body. The end result is an inertia tensor which will vary

slightly due to flexure of the solar panels and their repositioning. The main portion of the satellite is small and considered rigid.
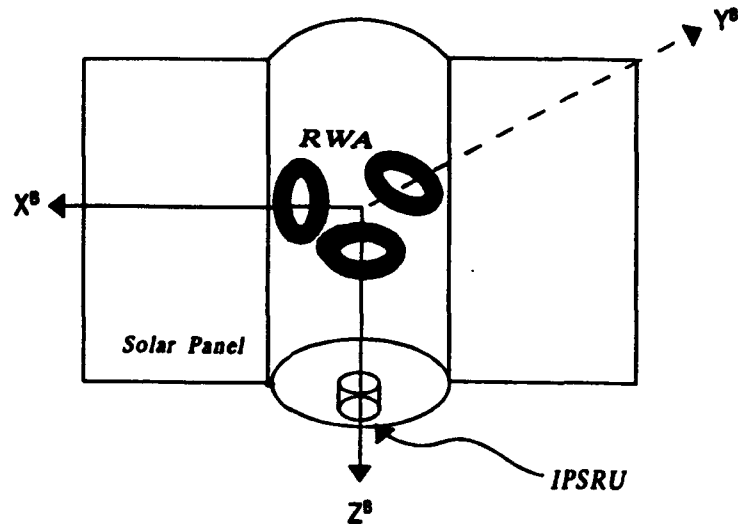
Figure 2-3: Spacecraft Configuration

The payload is assumed to be some type of optic, approximately 0.3 meters in diameter. The optic is rigidly mounted and aligned to the spacecraft. This is due to the advantageous use of IPSRU to provide the image stabilization, which in turn requires the satellite itself to be positioned to conduct imaging operations. The use of IPSRU allows for both a larger optic with higher resolution and the use of a non-articulated payload, which minimizes inertia tensor variations and additional rotational degrees of freedom.

After sizing of the other payload subsystems (e.g. power, thermal, communications subsystems) the spacecraft inertia tensor with the solar panels deployed preliminary estimate is [26]

$$J = \begin{bmatrix} 99.2 & 0 & 0 \\ 0 & 89.8 & 0 \\ 0 & 0 & 147.6 \end{bmatrix} \text{kg} \cdot \text{m}^2 \tag{2.7}$$

2.4.2 Attitude Determination and Control System Description

The attitude determination and control system is comprised of attitude sensors which determine the spacecraft orientation and actuators which affect the orientation to point towards a desired target. The attitude is determined from a combination of Sun and Earth sensors, gyroscopes, and star sightings from the optic which is used for calibration, as illustrated in Figure 2-4. The gyroscopes are considered the primary attitude sensors for this thesis although the other sensors will be used in the final configuration for redundancy and to reduce attitude uncertainty between calibrations using star sightings. For purposes of this thesis the attitude with respect to inertial space is assumed to have been calibrated and the gyroscopes are nearly perfect after filtering with the other attitude references. There are two gyroscopes—a two degree of freedom gyro mounted on IPSRU and one mounted on the spacecraft at the base of IPSRU. There are three orthogonally mounted reaction wheels which change the orientation of the spacecraft by changing the wheel speeds which exert a torque on the spacecraft. Magnetic torquers are used for momentum dumping of the reaction wheels, which is not included in the analysis of the control system here. Gas jets are available, but their primary purpose is orbit maneuvers for station-keeping and are not included in the control design either. Finally, a GPS receiver is assumed to be on the spacecraft, and is used to determine the orbital position, which is a key element of using on-board sensors for autonomous attitude determination.

The architecture shown in Figure 2-4 has three key functions: attitude determination and estimation from on-board sensors, calculation of the desired attitude based on target information, and determining the control inputs to the reaction wheels which affect the spacecraft orientation. As mentioned before, this thesis uses the IPSRU gyro and the spacecraft-mounted gyro as the primary attitude reference for the spacecraft. The IPSRU gyro is not fixed to the spacecraft body and IPSRU is mounted on a two degree-of-freedom flexure hinge whose angular displacement is measured; the spacecraft body rates in those two axes can be estimated from the angular displacement information and the gyroscope outputs as shown in Appendix D. The third axis rate is determined from the output of the gyro mounted to the spacecraft. The inertial attitude is then determined by integrating these rates and updating a direction cosine matrix which maps a vector from inertial to spacecraft body coordinates. Periodic recalibration of the gyroscopes is required as they tend to drift over time, although precise manufacturing
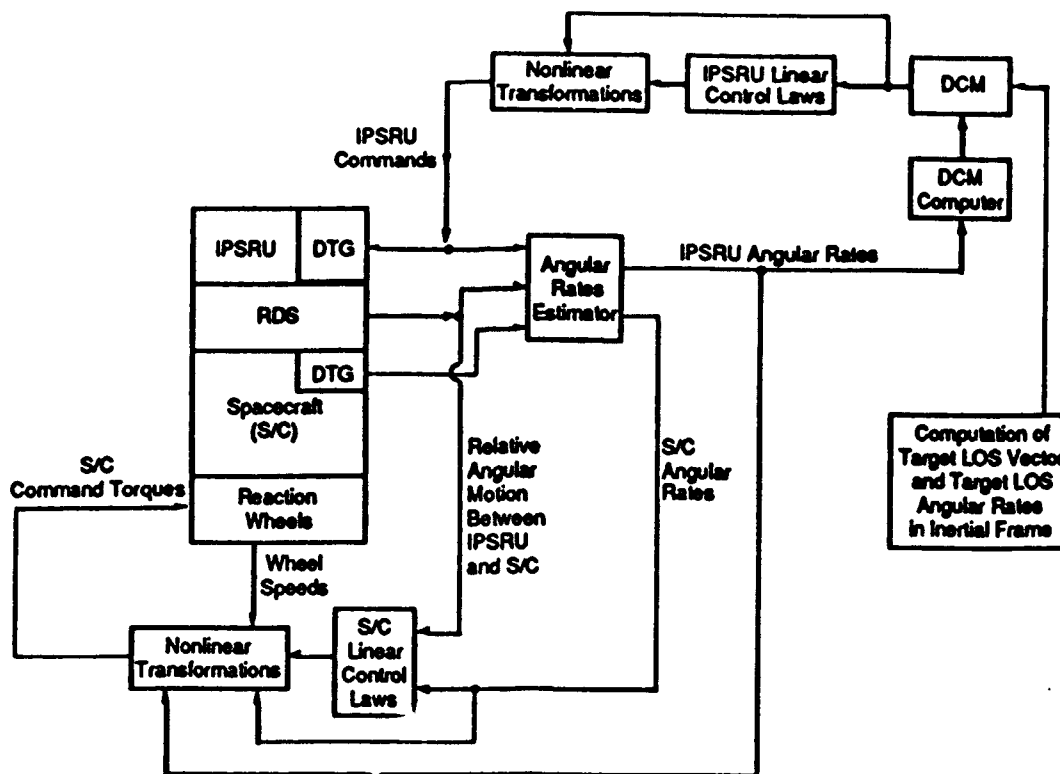
Figure 2-4: Attitude Determination and Control System Architecture

and testing can minimize this effect.

The desired attitute is determined by the use of on-board feedback and command inputs from desired target vector uplinks to the spacecraft. The method adopted here is to control the IPSRU platform such that the two components (direction cosines) of the target vector coordinatized in IPSRU platform coordinates go to zero, at which point the IPSRU reference beam LOS (z-axis) is automatically aligned with the target vector and the target will be acquired. This approach is similar to the spacecraft pointing approach adopted by many recent attitude determination schemes, such as those in [8], [12] and [27]. Quaternions are often favored over the use of direction cosines because of their computational advantages in determining the attitude of the vehicle, but direction cosines are adopted here because this advantage may not hold for control of a single vector (such as the IPSRU reference beam LOS) and also to facilitate intuition for the specification and performance analysis of the control system. The method adopted here only requires control of two direction cosine elements, whereas a quaternion parameterization

33

would require three, so the control computation may actually be less in this case. The direction cosine element paramaterization also permits straightforward kinematic and dynamical representations which are used in most dynamics texts. The desired target vector (which could be, for instance a target fixed to the Earth or simply a nadir pointing vector) is coordinatized into the IPSRU frame and is then compared to the direction cosine matrix of the IPSRU frame relative to inertial space; the error is then used to drive the IPSRU reference beam line of sight to line up the the IPSRU z-axis (reference LOS) with the target vector and maintain it there as derived in Appendix C. In this sense IPSRU is treated as a free body whose commands are the inputs to the gyroscopes. The inertial platform then starts to follow the commanded rates and generates an angular displacement which is used to determine the desired spacecraft rate and subsequent torque commands to the reaction wheels. This angular displacement cannot exceed 10 mrad, which are the limits of the flexure hinge.

The spacecraft control system must keep the angular displacement between IPSRU and the spacecraft small while resisting disturbances. The reaction wheels inputs are torque commands which are based on a desired spacecraft rate based on the IPSRU commanded rates and a feedforward command from the angular displacement. When the spacecraft controller is functioning properly, it should keep the displacement at null while the spacecraft rate matches the IPSRU commanded rate. The reaction wheels were sized to absorb the maximum disturbance torques (with margin) while maintaining the ability to slew the spacecraft at desired rates. The initial design includes a Draper Laboratory manufactured reaction wheel with the following characteristics [26]:

1. Angular momentum storage: 18.08 N · m.

2. Maximum torque output: 0.141 N · m · s.

3. Wheel speeds: -4200 to 4200 rpm.

4. Bandwidth: 0.5 Hz.

5. Axial Moment of Inertia: 0.0417 kg · m^2.

The maximum spacecraft angular rates can be approximated by using the reaction wheel maximum angular momentum, with the following assumptions:

1. The initial spacecraft total angular momentum is zero.

2. The reaction wheels are aligned perfectly along the principal axes of the spacecraft.

3. There is no internal energy dissipation.

Then the maximum rate along each axis is found by using the maximum angular momentum of the reaction wheel along that axis and transferring it to the total spacecraft system, or

$$\omega_{s/c\ max} = \frac{h_{rw\ max}}{I_{s/c\ axis}} \tag{2.8}$$

Using the inertias from Equation 2.7 in the above expression gives the following maximum angular rates of the spacecraft which can be imparted on a nonspinning vehicle: $\omega_x = 0.183$ rad/sec, $\omega_y = .201$ rad/sec and $\omega_z = 0.123$ rad/sec. If the spacecraft initially has angular momentum (such as tip-off rates from a booster or external torque effects), however, it is simpler to monitor the wheel speeds to ensure they do not reach saturation.

There are several aspects of the ACS subsystem which are not explored in this thesis. The initial detumble maneuver and additional Earth and Sun sensor filtering of attitude data are two examples. The thesis provides the basic architecture from which these and any other additional aspects of a complete spacecraft design can be engineered. The architecture may also realistically change as further studies progress and more definitive mission requirements are specified. The basic advantages of the IPSRU payload are incorporated into a preliminary architecture which will show potential application towards small, low-cost Earth observation satellite missions.

Chapter 3

Control Problem Formulation

Most spacecraft control texts describe control schemes which rely on some form of linear control design followed by simulation of the nonlinear equations of motion to determine performance. Even recent texts advocate this for many control designs, such as [1], [14] and [30]. This is usually adequate for a wide range of missions whose satellite attitude is either regulated towards nadir or do not require large angle slewing. These approaches also assume the vehicle is symmetric both in mass distribution and geometry, and in fact this can be achieved fairly accurately by deliberate manufacturing design of the spacecraft. Typical linear control designs include proportional/derivative (PD) control of the attitude parameterization, such as Euler angles or quaternions, or some form of passive stabilization such as the use of the mass properties of the vehicle to ensure one axis always points to nadir. These methods rely on the inherent physical properties of an earth-orbiting spacecraft such as the relatively disturbance free environment and conservation principles of the angular momentum and energy. The mission outlined here is typically accomplished from a 3-axis stabilized vehicle, which precludes passive techniques (as does the slewing requirement.) For large angle slewing requirements the linear design approach may work but the nonlinear coupling of terms in Euler's equation for a rotating body become more significant and off-axis errors and/or oscillations may induce attitude errors when attempting to point the spacecraft accurately. Other techniques not considered here are open loop pointing or control from ground stations, as the goal is to make the spacecraft autonomous other than uploading of desired target vectors. This leads to an approach using nonlinear control techniques to attempt to achieve better performance, especially in an autonomous mode.

The basic idea for this design was germinated by recent references on nonlinear feedback to achieve exact (or feedback) linearization ([8], [12], [23] and [27]). They all demonstrate the potential advantages for large slewing of spacecraft using direct spacecraft rate and attitude measurements to reorient a spacecraft. That approach is modified for this thesis to accomodate the use of sensors which are already available on the IPSRU platform, which saves cost,weight and power on the spacecraft bus at the expense of control complexity.

Approach

The approach to the overall control problem formulation was developed in steps, driven by the overall pointing objective. The first step was to determine how to point towards the target, which requires a method of determining the target vector (and vector motion) in relationship to the spacecraft attitude. The second step is to determine the strategy for controlling the spacecraft to follow the desired pointing. This "tail wagging the dog" approach is used because of the IPSRU purpose of stabilizing the image of the payload optic on the focal plane, as this requires the payload focal plane to be fixed to the spacecraft body. In essence the spacecraft must be slewed in order to point the payload at a desired target.

The target vector is assumed to be an earth-fixed target, whose coordinates are uploaded to the vehicle. The IPSRU inertial attitude is updated by integration of the IPSRU and spacecraft z-axis gyroscope as developed in Appendix D, so the target motion is coordinatized into the IPSRU frame and the IPSRU stable platform is commanded to follow the target unit vector by commanding the IPSRU x and y axes via rate command inputs. Thus IPSRU is treated as a free body and the control law is developed as a tracking problem.

The inputs to the IPSRU gyros are coordinatized into the spacecraft body frame by use of the direction cosine matrix which is calculated from the angular displacement between IPSRU and the spacecraft. The spacecraft is then controlled to follow the IPSRU commanded rates by control torque inputs to the reacton wheel assembly (RWA). This process is complicated by the requirement to keep the angular displacement less than 10 mrad, so a feedforward command is calculated based on the kinematics of the IPSRU platform in terms of the angular displacement motion. This feedforward command serves to regulate the angular displacement by anticipating the platform motion. If the displacement between the spacecraft and IPSRU is kept small, the

spacecraft body rate should closely match the IPSRU commanded rate and the results should be similar to those of Dwyer [8].

Feedback Linearization Technique

Feedback linearization as a control technique is used in the development of the control laws for both the IPSRU platform and the spacecraft, as will be seen in subsequent sections. The theory is not developed fully here, but a brief overview hopefully will provide some insight into the derivations in this chapter. First assume that a system is described by a nonlinear differential equation. The approach used in this thesis is to determine a nonlinear command input to a system such that any nonlinearities are canceled, resulting in a linear input/output mapping which can be used to form a linear control law for the controlled variable. Figure 3-1 illustrates the concept (and is adapted from [27]). The actual control input to the plant is then "recovered" to include the linear control of the actual controlled variable. If the model used in the inversion of the nonlinear plant parameters is exact, then the controlled variables should behave exactly like the linear plant; in practice any such coordinate change for the actual commands to the plant can result in restrictions on the controllable regions of the state space (a result of the plant inversion, or coordinate transformation). The control problem formulation of this chapter uses this approach to control the orientation of the IPSRU platform and the angular rate of the spacecraft, as will be shown in the control problem formulations.

3.1 Target Motion Analysis

The first step in the control process is to determine where the target is in relation to a known orientation of the vehicle. In this case the analysis is conducted in the IPSRU frame for convenience of matching the commanded IPSRU gyro rates and the IPSRU frame orientation in inertial space with the target unit vector coordinatized in IPSRU coordinates. The details of the target motion derivations are developed in Appendix C with this section provided as a summary to set the stage for the ISPRU control. The IPSRU frame is chosen as the coordinate frame for control of IPSRU as a free body to simplify the kinematic expressions in relation to the gyro command inputs which must be computed.
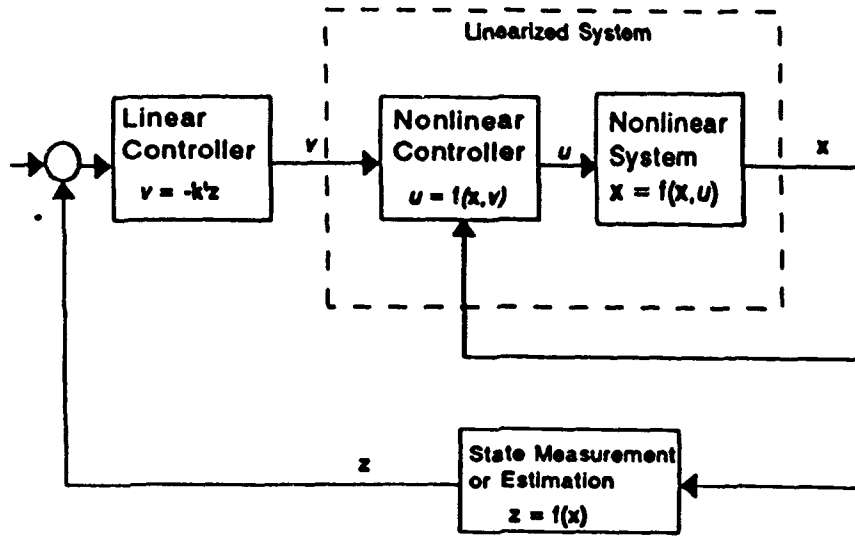
Figure 3-1: Exact Linearization Using Nonlinear Feedback

The assumptions are detailed in Appendix C, where the key assumptions are knowledge of the spacecraft orbit, the gyroscopes have been calibrated, and the direction cosine matrix which maps the vector from an inertial frame to the IPSRU frame has been computed and is being updated continuously from the gyro outputs. This DCM will use an intermediary ECI frame translation as described in Appendix B. The ECF to ECI coordinate transformation is known as well and the DCM which accomplishes this mapping is also continuously updated. The target vector is normalized and the resulting unit vector is designated $\underline{u}_T^I$, which is the target unit vector coordinatized in inertial coordinates. The DCM which maps this vector into IPSRU coordinates is designated C_I^P and the result is

$$\underline{u}_T^P = C_I^P \underline{u}_T^I \tag{3.1}$$

The unit vector will be time-varying, so the kinematics are simply expressed by differentiating both sides:

$$\underline{\dot{u}}_T^P = \frac{d}{dt}\left(C_I^P \underline{u}_T^I\right) \tag{3.2}$$

The right hand is expanded using the chain rule, and using the following kinematic relationship

39

$$\dot{\underline{u}}_T^I = \underline{\omega}_{IT}^I \times \underline{u}_T^I \tag{3.3}$$

along with some vector manipulations yields the following kinematic relationship:

$$\dot{\underline{u}}_T^P = \left(\underline{\omega}_{IT}^P - \underline{\omega}_{IP}^P\right) \times \underline{u}_T^P \tag{3.4}$$

Equation 3.4 is the basic kinematic equation describing the motion of the target vector in the IPSRU frame and forms the framework for the IPSRU control strategy developed in the next section. The terms in Equation 3.4 are defined as follows:

$\underline{u}_T^P$ is the target unit vector coordinatized in the IPSRU coordinate frame.

$\underline{\omega}_{IT}^P$ is the target rate with respect to the inertial frame in IPSRU coordinates.

$\underline{\omega}_{IP}^P$ is the IPSRU rate with respect to the inertial frame in IPSRU coordinates. Note the x and y components will be the inputs to the IPSRU gyro (assuming the stable platform responds perfectly to rate commands.)

The target rate vector and the target unit vector are computable on-board the spacecraft as outlined in Appendix C. For the remainder of the thesis the z-axis target rate will be assumed to be zero, as one would expect it to be undesirable for the target to turn around the line of sight. Additionally, the following notation definitions are used to simplify complexity of the equations:

$$\underline{u}_T^P \equiv \underline{u}_T$$

$$\underline{\omega}_{IT}^P \equiv \underline{\omega}_T$$

$$\underline{\omega}_{IP}^P \equiv \underline{\omega}_P$$

$$\underline{u}_{T_{x,y,z}}^P \equiv u_{x,y,z} \text{ (components of the unit target vector)}$$

$$\underline{\omega}_{IT_{x,y,z}}^P \equiv \omega_{T_{x,y,z}} \text{ (components of the target rate vector)}$$

$$\underline{\omega}_{IP_{x,y,z}}^P \equiv \omega_{P_{x,y,z}} \text{ (components of the IPSRU rate vector)}$$

The full notation may be used where potential ambiguities may exist.

40

3.2 IPSRU Control Under Ideal Assumptions

The control sytem objective is to accurately point the unit vector of the IPSRU reference beam LOS. This unit vector must accurately move from one target to another and once at the target must follow the target motion. The unit vector $\underline{u}_T^P$ is restricted in magnitude, so control of the unit vector x and y axes controls the third axis via the constraint

$$u_z = \sqrt{1 - u_x^2 - u_y^2} \tag{3.5}$$

Thus by controlling u_x and u_y with $\omega_{P_{x,y}}$ as the control inputs, the platform may be oriented to line up with the target, as shown in Figure 3-2. This technique is is similar to tactical missile guidance control of the azimuth and elevation (and perhaps their rates and/or accelerations) of the target with respect to the missile [6]. The differential equations governing the two axes are determined by calculating the scalar equations from Equation 3.4:

$$\dot{u}_x = \omega_{T_y} u_z + \omega_{P_z} u_y - \omega_{P_y} u_z \tag{3.6}$$

$$\dot{u}_y = -\omega_{T_x} u_z - \omega_{P_z} u_x + \omega_{P_x} u_z \tag{3.7}$$

The control problem is to determine commands to the IPSRU gyros (ω_{P_i}) such that u_x and u_y go to zero. This means that the unit vector in the z direction has a magnitude of 1 and points toward the target. In addition, $\dot{u}_x$ and $\dot{u}_y$ must go to zero in order for the IPSRU reference beam LOS to follow the target vector coordinatized in the IPSRU frame. Additionally, there are restrictions on the rate and acceleration commmands that control IPSRU, in terms of physical limits on the actuators and the IPSRU unit itself. Finally, there is an effect of any IPSRU control inputs on the spacecraft control inputs to the reaction wheels, which themselves are physically limited.

Inspection of Equations 3.6 and 3.7 reveals that the equations are nonlinear and coupled— thus in order to use the powerful tools of linear control system design some method of linearization (under reasonable assumptions) must be applied to the system model. The use of feedback linearization is used in this analysis because of its potential advantage in large angle slews, at

41
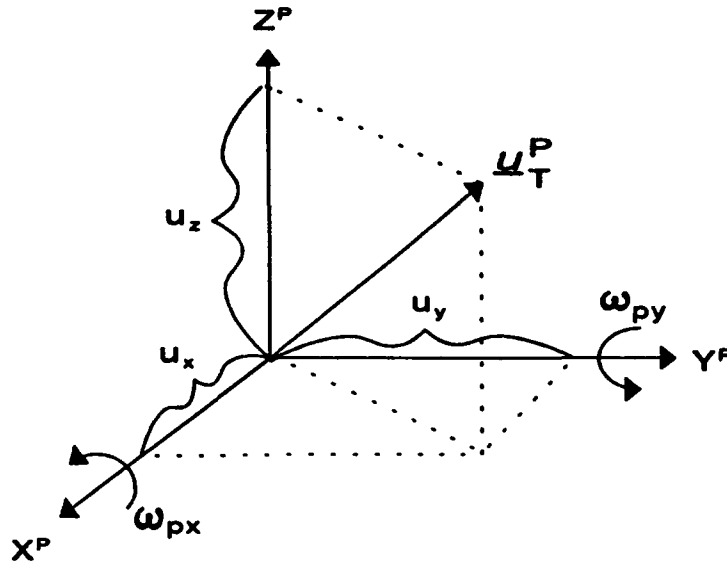
Figure 3-2: Target Unit Vector in the IPSRU Platform Frame

the disadvantage of not having the strong analytical/empirical base that linearizing about an operating point has for stability analysis. Intuitively, after the linearization process, the use of some form of optimal control to effectively minimize the energy of the reaction wheels seemed appropriate. Thus several optimal control designs using a quadratic cost penalty function were compared.

3.2.1 Proportional Control of u_x and u_y

Equations 3.6 and 3.7 above can be linearized by a very simple transformation [22]:

$$\dot{u}_x = v_x \tag{3.8}$$

$$\dot{u}_y = v_y \tag{3.9}$$

In this form the control equations are scalar and uncoupled and a control law for each of the

axes can be designed separately. The actual control law can then be recovered by solving for the IPSRU commands in Equations 3.6 and 3.7 and substituting the control law in for $\dot{u}_i$.

Cost Function

The control problem is formulated in terms of a quadratic cost function with the desire to place a penalty on the final values of $\dot{u}_x$, $\dot{u}_y$, u_x and u_y, because at the final time the desire is to have acquired the target and to begin tracking it (either open loop pointing or closed-loop, depending on the payload mission). However, the desire to limit control authority requires a penalty on the control effort; thus a suitable cost function is

$$ J = su_i^2(t_f) + \int_{t_0}^{t} \rho v_i^2(t)dt \tag{3.10} $$

where

1. The term s is the weight on the final state.

2. The term u_i is the ith axis state as described above.

3. The term ρ is the weight on the control (from now on this will be set to the value "1" to simplify the derivations.)

4. The term v_i is the ith axis control.

The following derivations will only be for the x-axis; this is because the linearized equations are uncoupled and a similar derivation can be done for the y-axis.

Derivation of the Control

The Riccati equation for the cost function above is

$$ \dot{\Pi}(t) = -\Pi^2(t), \quad \Pi(t_f) = s \tag{3.11} $$

whose solution is [9]:

$$ \Pi(t) = \frac{1}{(t_f - t) + \frac{1}{s}} \tag{3.12} $$

43

The optimal control for this system will be of the form

$$v_x^*(t) = -k(t)u_x(t) \qquad (3.13)$$

where k(t) is a function of the solution to the Riccati equation

$$k(t) = B^T \Pi(t) \qquad (3.14)$$

The system in closed loop form using the above optimal control is

$$\dot{u}_x(t) = -\frac{1}{(t_f - t) + \frac{1}{s}} u_x(t) \qquad (3.15)$$

The solution for this equation is of the well-known form [6]:

$$u_x(t) = u_x(t_0) e^{\int_{t_0}^{t} -k(\tau)d\tau} \qquad (3.16)$$

Calculating the integral gives the solution

$$u_x(t) = u_x(t_0) \left(\frac{t - (t_f + \frac{1}{s})}{t_0 - (t_f + \frac{1}{s})} \right) \qquad (3.17)$$

Taking the derivative with respect to t gives the final result:

$$\dot{u}_x(t) = u_x(t_0) \frac{1}{t_0 - (t_f + \frac{1}{s})} \qquad (3.18)$$

Analysis of the Proportional Control

The control method used above yields a control law which will always have an error in the final state for u_x. When the control is substituted back into Equation 3.6 and ω_{Bx} is solved for, this translates to the commanded input not matching the target rate. Increasing the control gains can result in potentially acceptable errors at the expense of higher rates. Another disadvantage of this method is that the acceleration will be uncontrollable, which forces empirical testing. However, the method is attractive from the standpoint of simplicity.

44

3.2.2 Second Order Fixed-Time Control of IPSRU

Section 3.2.1 outlined an approach that was attractive for its simplicity, with a disadvantage of the inability to control the IPSRU rate command. One way to approach it along the same methodology is to use control the rate of change of the unit target vector as well, essentially PD control. Now the linearized system of equations includes the derivatives of the proportional control method's linearized equations, resulting in

$$
\begin{aligned}
\dot{u}_x &= v_x \\
\dot{v}_x &= s_x \\
\dot{u}_y &= v_y \\
\dot{v}_y &= s_y
\end{aligned}
\tag{3.19}
$$

Once again, the linearized equations are scalar and are uncoupled. This formulation allows control of $\dot{u}_x$ and $\dot{u}_y$, allowing them to be driven to zero. The result is the target rate matches the IPSRU commanded rate at the time of target acquisition.

One state-space representation of this system (for the x axis) can be established as follows:

$$
\begin{aligned}
x_1 &= u_x \\
x_2 &= \dot{x}_1 \\
\dot{x}_2 &= w_x
\end{aligned}
$$

which results in a state-space representation of the form

$$
\underline{\dot{x}} = A\underline{x} + Bw
\tag{3.20}
$$

where the actual values are

$$\begin{bmatrix} \dot{x}_1 \\ \dot{x}_2 \end{bmatrix} = \begin{bmatrix} 0 & 1 \\ 0 & 0 \end{bmatrix} \begin{bmatrix} x_1 \\ x_2 \end{bmatrix} + \begin{bmatrix} 0 \\ 1 \end{bmatrix} w \tag{3.21}$$

Cost Function

The same approach is adopted as in section 3.2.1 for the determination of the cost function—the only difference is the state-space is no longer scalar and the quadratic weight is a matrix. For a fixed-time optimal control problem with penalties on the final states and limitations on the control effort, the cost function is [6]:

$$J = \underline{x}^T(t_f) S \underline{x}(t_f) + \int_{t_0}^{t} \underline{w}^T(t) R \underline{w}(t) dt \tag{3.22}$$

Once again, this cost function places weights on the final state and control, but not the trajectory. Note the state and control are defined in Section 3.2.2.

Derivation of the Control

The Riccati equation associated with the cost function above is a differential matrix Riccati equation of the form

$$\dot{\Pi}(t) = -\Pi(t)A - A^T\Pi(t) + \Pi(t)B^T B\Pi(t), \quad \Pi(t_f) = S^{-1} \tag{3.23}$$

The solution to the inverse of $\Pi(t)$ given S and R can be computed [9]:

$$\begin{aligned}
p^1(t) &= \frac{1}{3}(t_f - t)^3 + \frac{1}{s_2}(t_f - t)^2 + \frac{1}{s_1} \\
p^2(t) &= \frac{1}{2}(t_f - t)^2 - \frac{1}{s_2}(t_f - t) \\
p^3(t) &= (t_f - t) + \frac{1}{s_2}
\end{aligned}$$

These elements form the matrix $\Pi^{-1}(t)$, which must be inverted in order to find the solution to the Riccati equation:

46

$$\Pi(t) = (\Pi^{-1}(t))^{-1} = \frac{\begin{bmatrix} p^1(t) & p^2(t) \\ p^2(t) & p^3(t) \end{bmatrix}}{p^3(t)p^1(t) - (p^2(t))^2} = \begin{bmatrix} p_1(t) & p_2(t) \\ p_2(t) & p_3(t) \end{bmatrix} \qquad (3.24)$$

The optimal control is then given by

$$w^*(t) = -B^T\Pi(t)\underline{x}(t) \equiv -K(t)\underline{x} \qquad (3.25)$$

When the actual matrices B^T and $\Pi(t)$ are multiplied, the result is

$$w^*(t) = -k_1(t)x_1 - k_2(t)x_2 = -p_2(t)x_1 + -p_3(t)x_2 \qquad (3.26)$$

Substituting $w^*(t)$ into the original system equation 3.21 results in the closed loop system

$$\underline{\dot{x}} = [A - BB^T\Pi(t)]\underline{x}(t) \qquad (3.27)$$

whose solution is of the form

$$\Phi(t, t_0) = e^{\int_{t_0}^{t}[A-BB^T\Pi(\tau)]d\tau} \qquad (3.28)$$

Now define

$$ACL(t) = A - BB^T\Pi(t) = \begin{bmatrix} 0 & 1 \\ -p_2(t) & -p_3(t) \end{bmatrix} \qquad (3.29)$$

Using the original state variable names results in the following closed loop response:

$$\begin{bmatrix} u_x(t) \\ \dot{u}_x(t) \end{bmatrix} = e^{\int_{t_0}^{t} ACL(\tau)d\tau} \begin{bmatrix} u_x(t_0) \\ \dot{u}_x(t_0) \end{bmatrix} \qquad (3.30)$$

Unlike the proportional method of control, the solution to the state transition equation is not easily found analytically so is numerically integrated to determine the ideal linear system closed loop response.

Calculating ω_{P_i}

The linear equations used to derive the above system of equations is based on exact linearization by using nonlinear feedback. Recall the control variables in the nonlinear equations are ω_{P_x} and ω_{P_y}, which are the commanded inputs to the IPSRU two degree of freedom gyro. Under the idealizing assumptions that all of the coordinate frame axes are exactly lined up and the platform responds perfectly to these rate commands, it is possible to calculate ω_{P_x} and ω_{P_y} such that the nonlinear terms are canceled. The result is a computed gyro input which provides the desired linear input-output response for the control of u_x and u_y. The linearization of the original control equations is accomplished by setting the whole right half side of the equations (the nonlinear portions) to a scalar. The nonlinear transformations to determine the IPSRU commands which accomplishes this under these assumptions are:

$$\omega_{P_x} = \omega_{T_x} + \frac{v_y + \omega_{P_z} u_x}{u_z} \tag{3.31}$$

$$\omega_{P_y} = \omega_{T_y} - \frac{v_x - \omega_{P_z} u_y}{u_z} \tag{3.32}$$

Recall $u_z = \sqrt{1 - u_x^2 - u_y^2}$, so the transformation above is nonlinear. In addition, notice the cross coupling of the axes—this is due to the cross-coupling in commanding the gyroscope to torque about each axis. Because u_z is in the denominator, it cannot get too close to zero. Methods of working around this restriction are described in [22], whereby an intermediate trajectory is picked when u_z gets small or a nonlinear function of u_z (e.g. dead-zone nonlinearity) is used in the control equation to avoid cases where u_z gets too small. For this thesis, the condition is avoided by limiting the maximum slew angle to approximately 70 degrees, which should adequately meet nearly all mission requirements.

Calculating ω_{P_i} Ignoring Nonlinearities

The controller design from the previous section requires effectively that a plant inversion must be calculated in order to cancel the nonlinear terms via the nonlinear feedback. The nonlinear terms and cross coupling terms are expected to be small, so a simpler approach would be to simply ignore those terms and design a linear controller; this is a typical method of spacecraft

48

regulator control [14]. Assuming this controller was robust, it would then be adequate to compensate for the small nonlinear parametric uncertainties and dynamics.

Using this method, the linear control equations (for the x axis) are simply:

$$\dot{u}_x \;=\; \omega_{P_y} \tag{3.33}$$

$$\dot{\omega}_{P_y} \;=\; s_x \tag{3.34}$$

Now this system of equations generates a linear control law s_x, which is integrated to determine ω_{P_y} which in turn is substituted as the control input in the original kinematic equations, resulting in

$$\dot{u}_x = \omega_{T_y} u_z + \omega_{P_z} u_y - \omega_{P_y} u_z \tag{3.35}$$

Simplifying the above equation in terms of u_x and u_y yields

$$\dot{u}_x = (\omega_{T_y} - \omega_{P_y})\sqrt{1 - u_x^2 - u_y^2} + \omega_{P_z} u_y \tag{3.36}$$

Using the same approach for the y axis yields a similar result:

$$\dot{u}_y = (\omega_{P_x} - \omega_{T_x})\sqrt{1 - u_x^2 - u_y^2} - \omega_{P_z} u_x \tag{3.37}$$

The two equations are nonlinear and coupled, and the solution to the equations is found by numerical integration. Since each term is norm-bounded it is expected for the system to be bounded (in terms of rate).

3.2.3 Gyroscope Measurements and the Control of IPSRU

The computed control inputs to the IPSRU gyros in Equations 3.31 and 3.32 are based on knowledge of the rates of the IPSRU platform in all three axes. The z-axis gyro, however, is mounted to the spacecraft and therefore the measurement cannot be used directly in computing the control. Appendix D derives a method for estimating the IPSRU platform rates using all three gyros:

$$\underline{\omega}_{IP}^{P} = \begin{bmatrix} \omega_{P_x} \\ \omega_{P_y} \\ \omega_{B_z} + \theta_y \omega_{P_x} - \theta_x \omega_{P_y} + \theta_y \dot{\theta}_x \end{bmatrix} \tag{3.38}$$

where

ω_{B_z} = the spacecraft z-axis output (component of the spacecraft rate $\underline{\omega}_{IB}^{B}$).

$\theta_{x,y}$ = angular displacement angles between the IPSRU platform and the spacecraft.

There is a problem in using the result as stated above because the computation of the z-axis IPSRU rate is based on the IPSRU x and y axes rates, which is a "catch-22" situation because the goal is to determine how to use the z-axis gyro to compute those rates when computation of the z-axis gyro rate coordinatized into the IPSRU frame requires knowledge of the IPSRU x and y rates. However, an approximation to the exact linearization is developed in Appendix D, resulting in an approximation to the exact linearization of the IPSRU computed control by directly using the spacecraft z-axis gyro rate as follows:

$$\begin{bmatrix} \omega_{P_x} \\ \omega_{P_y} \end{bmatrix} = \frac{1}{u_z} \begin{bmatrix} u_z + \theta_y u_x & -\theta_x u_x \\ \theta_y u_y & u_z - \theta_x u_y \end{bmatrix} \begin{bmatrix} \omega_{T_x} + \frac{v_y}{u_z} + \frac{\omega_{B_z} u_x}{u_z} \\ \omega_{T_y} - \frac{v_x}{u_z} + \frac{\omega_{B_z} u_y}{u_z} \end{bmatrix} \tag{3.39}$$

Figure 3-3 illustrates the overall approach to compute the IPSRU commands.

3.3 Idealized Spacecraft and Reaction Wheel Assembly Equations of Motion

The following derivation closely follows any classical derivation of Euler's equations for a rotating rigid body, with the exception of the internal degree of freedom for the three orthogonally mounted reaction wheels. The basic assumptions are

1. The spacecraft is a rigid body.

2. The reaction wheels are perfectly orthogonal and are aligned along the spacecraft principle moments of inertia.

50
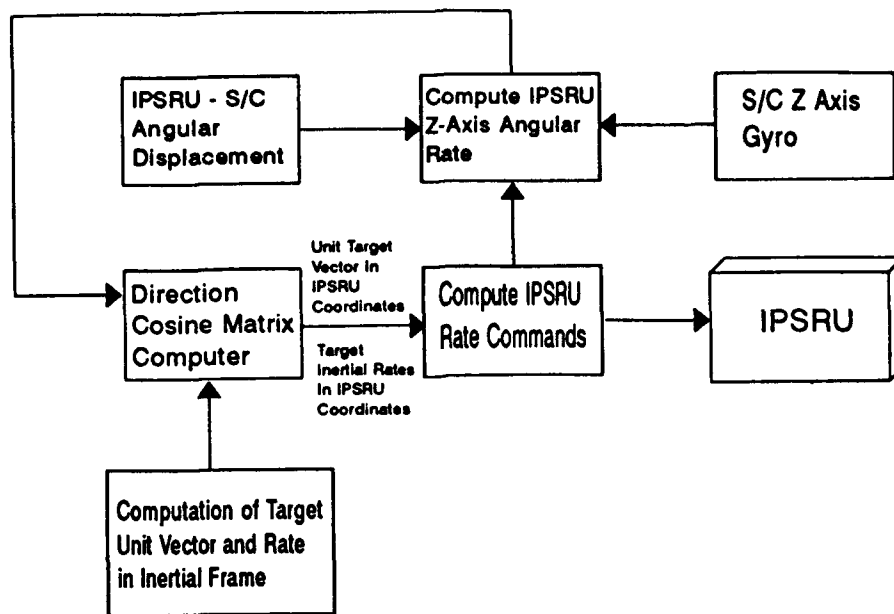
Figure 3-3: Computation of IPSRU Commands

3. There are no external torques acting on the spacecraft.

4. The reaction wheels respond perfectly to control torque inputs.

Additionally, there are limits on the angular momentum of the reaction wheels and the torque outputs, but generally those will be ignored until the control law as been analyzed. This derivation closely follows the derivation of Junkins and Turner [13]. Similar results can be found in many texts, including [11], [14], and [30]. The ultimate goal is to determine an expression for the angular rates of the spacecraft body as a function of the control torque command to the reaction wheel assembly, in order to determine how to command the spacecraft rates to follow the IPSRU commanded rates.

The coordinate frame used in the derivations is a body-fixed orthogonal frame, with the body coordinates center at the center of mass and the axes aligned along the directions of the principle moments of inertia. The angular rate vector of the body with respect to inertial space coordinatized in the body frame is $\underline{\omega}_{IB}^{B}$. For the remainder of this section the notation will be

simplified to ω_B with the x, y and z components of the vector represented as ω_{Bx}, ω_{By} and ω_{Bz}. The angular momentum vectors of both the spacececraft and reaction wheels are also assumed to be coordinatized in the body frame.

The first step is to express the total angular momentum of the composite body in terms of the angular momentum of the spacecraft and the angular momentum of the reaction wheels:

$$\underline{h}_{total} = \underline{h}_{s/c} + \underline{h}_{wheels} \tag{3.40}$$

Now, using the general relationship

$$\underline{h}_{total} = J\underline{\omega}_B$$

where J is the composite inertia tensor of the spacecraft and reaction wheels and $\underline{\omega}_B$ is the angular rate vector of the body coordinatized in the body frame, results in the standard dynamic equation of rotational motion [13] as follows. For notational convenience, let $\underline{h}_{wheels} = \underline{h}$. The derivative of $\underline{h}_{total}$ with respect to the inertial frame is composed of the rate of change of $\underline{h}_{total}$ in the body frame plus the cross product of the angular rate with the angular momentum vector:

$$\dot{\underline{h}}_{total} = J\dot{\underline{\omega}}_B + \underline{\omega}_B \times J\underline{\omega}_B \tag{3.41}$$

Substituting Equation 3.40 into Equation 3.41 results in

$$\dot{\underline{h}}_{total} = J\dot{\underline{\omega}}_B + \dot{\underline{h}} + \underline{\omega}_B \times (J\underline{\omega}_B + \underline{h}) \tag{3.42}$$

The total change of angular momentum is conserved in the absence of external torques, so $\dot{\underline{h}}_{total} = 0$. Thus Equation 3.42 can be rearranged:

$$J\dot{\underline{\omega}}_B + \dot{\underline{h}} = -\underline{\omega}_B \times (J\underline{\omega}_B + \underline{h}) \tag{3.43}$$

At this point the term an expression for the motor torque input to a single reaction wheel is considered. First, denote the axial moment of inertia for any wheel as I_a. Also assume that the wheels are rigid and axisymmetric, so the transverse components of the wheel inertia principle axes, I_t, are equal. The motor torque is comprised of the body angular acceleration

52

acting around the axial angular momentum vector along with the rate of change of the angular momentum of the wheel with respect to the body ($\dot{h}$). Note that the angular momentum of the wheel with respect to the body is a function of the angular rate of the wheel speed, w:

$$h = I_a w$$

Thus the motor torque acting on any reaction wheel along a particular component of the body-frame unit vector direction is governed by [13]:

$$\tau(t) = I_a(\dot{\omega}_{Bi} + \dot{w}) = I_a\dot{\omega}_{Bi} + \dot{h} \tag{3.44}$$

Now solve for $\dot{h}$ in Equation 3.44:

$$\dot{h} = -I_a\dot{\omega}_{Bi} + \tau(t) \tag{3.45}$$

This expression can then be used in a matrix and vector formulation as follows. Denote the diagonal matrix J_a as the matrix with the axial inertia moments of each wheel along the diagonal. The vector relation is then

$$\underline{\dot{h}} = -J_a\underline{\dot{\omega}}_B + \underline{\tau} \tag{3.46}$$

Substituting Equation 3.46 into Equation 3.43 and rearranging so all the terms with $\underline{\dot{\omega}}_B$ appear on the left-hand side:

$$J\underline{\dot{\omega}}_B - J_a\underline{\dot{\omega}}_B = -\underline{\omega}_B \times (J\underline{\omega}_B + \underline{h}) - \underline{\tau} \tag{3.47}$$

Now denote the matrix $A = J - J_a = J_{s/c} + 2I_t I_3$, where I_t is the transverse moment of inertia for each wheel and I_3 is the 3×3 identity matrix. Thus, a first order differential equation for the angular rates of the spacecraft is obtained:

$$\underline{\dot{\omega}}_B = A^{-1}\left[-\underline{\omega}_B \times (J\underline{\omega}_B + \underline{h}) - \underline{\tau}\right] \tag{3.48}$$

Equation 3.45 provides the additional state equation to complete the system of equations which will be used to determine the control strategy for the spacecraft. Note that these equations in the matrix/vector formulation are more general than the scalar equations used by Junkins [13], which will be exploited for some of the error analysis due to plant uncertainties.

3.4 Spacecraft Control Under Ideal Assumptions

The approach for the spacecraft control is similar to the IPSRU platform control, as the plant is invertible since the inertia tensor matrices A and J will be positive definite and rank 3. Intuitively, because of the relatively isolated dynamics of the spacecraft and the well-known stability properties and performance limitations, the use of feedback linearization should prove to be effective and hopefully will produce a significant gain in performance. Since most spacecraft maintain a fixed or slowly moving orientation with respect to inertial space, actual linear controllers are typically implemented and prove effective for small deviations, and in fact most modern texts (for example [11], [14] and [30]) typically advocate ignoring the coupling terms and designing control of each axis assuming they are a set of decoupled linear equations, followed by nonlinear simulations to tune the controller. Larger, more flexible spacecraft structures and increased demands on smaller spacecraft in terms of rapid large angle slewing, combined with increasing performance requirements have led to the application of more advanced nonlinear control techniques, one of which is feedback linearization which will be applied here. This analysis is related to recent references in spacecraft controls literature such as [7], [8], [13] and [23].

This technique is feasible for the system model represented by Equation 3.48 because the ideal plant is invertible in terms of the motor torque input to the reaction wheels:

$$\underline{\tau} = A^{-1} \left[-\underline{\omega}_B \times (J\underline{\omega}_B + \underline{h}) - A\underline{m} \right] \tag{3.49}$$

where $\underline{m}$ is the control on the desired spacecraft rate. When the computed torque is of this form, Equation 3.49 is substituted into Equation 3.48 to form three sets of decoupled control equations in each axis in terms of the desired angular acceleration, $\underline{\dot{\omega}}_B$:

$$\dot{\omega}_{Bx} = m_x$$
$$\dot{\omega}_{Bx} = m_y \tag{3.50}$$
$$\dot{\omega}_{Bx} = m_z$$

The goal of the "linear" spacecraft controller for the x and y axes in this formulation is to follow a commanded rate which is essentially the IPSRU commanded rate coordinatized into the spacecraft coordinate frame along with a feedforward command based on the kinematics of the IPSRU platform which will keep the displacement between IPSRU and the platform less than 10 mrad. The z axis must follow the desired angular rate which is the IPSRU z-axis rate coordinatized in the body frame, or $\omega_{P_z}^B$.

3.4.1 Desired Spacecraft Rates

The linear controllers for the decoupled linearized equations above must accomplish two design objectives. First, they must track the rate commands to the IPSRU platform (coordinatized in the body frame.) At the same time, they must follow the IPSRU platform motion by regulating the angular displacement between the platform and the s/c body. The z axis rate must be regulated to zero to prevent turning of the target about the line of sight as well. The design for the controllers outlined here assumes the reaction wheels are ideal, e.g. they respond to the desired commands instantaneously.

Approach

The approach adopted here is sequential, which allows for straightforward design of several control loops which when assembled in final form will meet the design objectives. The first is the design of a regulator for the angular displacement of the IPSRU platform from the spacecraft body, which requires development of the platform kinematics based on the flexure hinge gimbals and platform rates which will be used to compute feedforward commands to the reaction wheels which will cancel (regulate) the effects of spacecraft and IPSRU motion on the angular displacement. These same angular displacements are then used to determine the

direction cosine matrix which transforms the IPSRU commanded rates into spacecraft body rates in the form of reference variables, or tracking commands. Additionally, the direction cosine transformation is used to estimate the spacecraft x and y axis rates for use in the overall feedback control. The z-axis gyro will be used to estimate the spacecraft desired z-axis rate *indirectly* as its measurement is cross-coupled in the kinematics as shown in Equation 3.7.

Regulating the Angular Displacement

The first step in this process is to determine an expression which describes the motion of the platform in terms of θ_x and θ_y, which are the angular displacement measurements for the platform. The basic derivation of this motion developed in Appendix D is based on using the small angle approximations

$$\sin \theta \cong \theta$$

$$\cos \theta \cong 1$$

$$o(\theta) \cong 0 \text{ (e.g. second order and h.o.t.)}$$

because the *maximum* platform displacement is 10 mrad and should be much less for conservative design (5 mrad). Justification for this approximation is also described in Appendix D. Additionally, the following assumptions are used in the derivation:

1. The IPSRU platform is a rigid body.

2. The platform flexure hinges are located at the center of the coordinate system, which are aligned along symmetric axes.

3. There is no displacement about the z-axis.

4. The angular displacements are measured perfectly and the angular displacement rates are computable either by approximate differentiation or some other method of accurate filtering.

The direction cosine matrix which maps a vector coordinatized in the IPSRU frame into the s/c body frame is found by rotating the body frame coordinate frame around the x-axis and

56

then the y-axis (this could also be accomplished through a y-x axis rotation transformation.) The result is

$$C_P^B = \begin{bmatrix} \cos\theta_y & \sin\theta_x \sin\theta_y & -\sin\theta_y \cos\theta_x \\ 0 & \cos\theta_x & \sin\theta_x \\ \sin\theta_y & -\sin\theta_x \cos\theta_y & \cos\theta_x \cos\theta_y \end{bmatrix} \cong \begin{bmatrix} 1 & 0 & -\theta_y \\ 0 & 1 & \theta_x \\ \theta_y & -\theta_x & 1 \end{bmatrix} \quad (3.51)$$

The platform kinematics in terms of the s/c body frame coordinates are derived using the same basic approach as the IPSRU reference beam target LOS control. In this case the goal is to command the unit vector which represents the z-axis of the IPSRU coordinate frame in s/c body coordinates to line up with the spacecraft body frame z axis by rotating the s/c body frame. The IPSRU frame z-axis is denoted $\underline{z}^P$, so using the DCM yields the unit vector which must be controlled in the spacecraft body frame, $\underline{u}_{zP}^B$, which is analagous to the IPSRU target unit vector $\underline{u}_T^P$. The kinematics of the platform in s/c coordinates is then found by using the same approach as the IPSRU target kinematics:

$$\underline{\dot{u}}_{zP}^B = \frac{d}{dt}\left[C_P^B \underline{z}^P\right] \quad (3.52)$$

which when simplified in Appendix D by using small angle approximations and kinematics yields two first order differential equations which describe the motion of the IPSRU platform in spacecraft coordinates in terms of the angular displacements and rates:

$$\dot{\theta}_x = -\omega_{B_x} - \theta_y\left(\omega_{P_z}^B - \omega_{B_z}\right) + \omega_{P_x} \quad (3.53)$$

$$\dot{\theta}_y = -\omega_{B_y} + \theta_x\left(\omega_{P_z}^B - \omega_{B_z}\right) + \omega_{P_y} \quad (3.54)$$

The regulation of θ_x and θ_y can be derived first by using the following decoupled linear state equations (for the x axis only, the y axis is derived similarly):

$$\dot{\theta}_x = \phi_x \quad (3.55)$$

57

$$\dot{\phi}_x = q_x \qquad (3.56)$$

which, like the IPSRU target unit vector control, is essentially a full-state double integrator system and represents the desired linear system from a modeling standpoint. Then a linear control can be found of the form

$$q_x = -k_3\,\theta_x - k_4\,\dot{\theta}_x \qquad (3.57)$$

which will regulate the angular displacement to zero. To determine the feedforward control, the identity

$$\phi_x = \int_{t1}^{t2} q_x\, dt \qquad (3.58)$$

is substituted into Equation 3.53, and the feedforward command is solved for as the desired rate $\tilde{\omega}_{B_x}$. The desired feedforward command for the y axis is solved for similarly and the results are feedforward commands for both the x and y axes. Additionally, the desired rate for the z axis is ω_{B_z}. Thus, the desired rates which the spacecraft must follow are

$$\tilde{\omega}_{B_x} = -\phi_x - \theta_y \left(\omega_{P_z}^B - \omega_{B_z}\right) + \omega_{P_x} \qquad (3.59)$$

$$\tilde{\omega}_{B_y} = -\phi_y + \theta_x \left(\omega_{P_z}^B - \omega_{B_z}\right) + \omega_{P_y} \qquad (3.60)$$

$$\tilde{\omega}_{B_z} = \omega_{P_z}^B \qquad (3.61)$$

This process is illustrated in Figure 3-4.

Estimating the IPSRU Rates in the Spacecraft Body-Fixed Frame

Equations 3.59—3.61 require knowledge of the IPSRU rates coordinatized into the spacecraft frame. A method for estimating these rates is summarized in Appendix D (from [22]) and is based on small angle approximations and caculating the first order differential equations for each gimbal of the flexure hinge. The order of the gimbals does not matter using the small angle approximations, but is important if they are not used, in which case the same axis rotations as
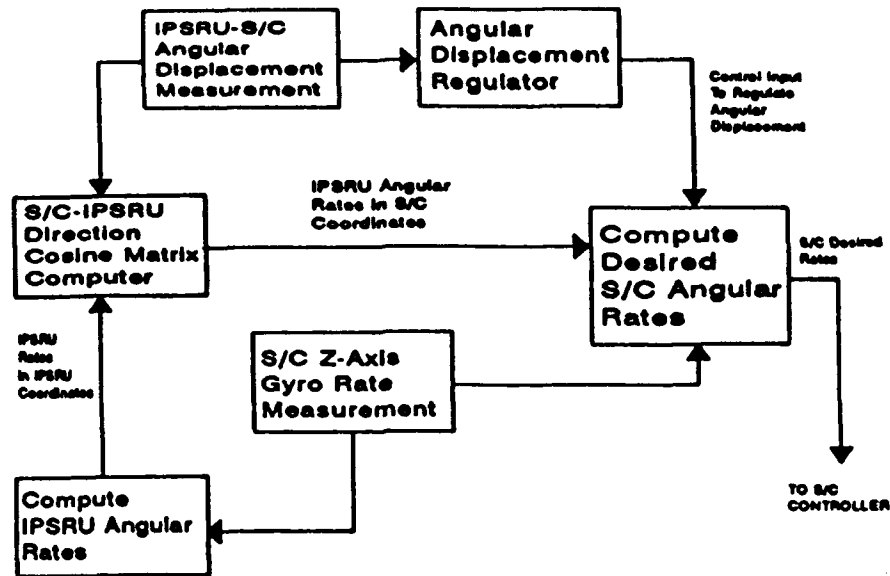
Figure 3-4: Calculating the Desired Spacecraft Angular Rates

the DCM C_P^B is required. The result using this method is

$$\dot{\omega}_{IB}^B = \begin{bmatrix} \omega_{P_x} + \theta_y \omega_{B_x} - \dot{\theta}_x \\ \omega_{P_y} - \theta_x \omega_{B_z} - \dot{\theta}_y \\ \omega_{B_z} \end{bmatrix} \tag{3.62}$$

Inspection of Equation 3.62 with Equations 3.53 and 3.4.1 demonstrates it should yield a good approximation for the rates, especially as the term $\omega_{P_z}^B$ should get vanishingly small for small values of θ_x, θ_y, and ω_{B_z}.

3.4.2 Calculation of the Control Torque Input to the RWA

The control torque inputs to the reaction wheels are first found by solving a linear control law for the desired input/output linear response dictated by Equation 3.50. A simple asymptotic tracking law would be a negative feedback gain of the form

$$\underline{m} = -K_5 \left(\underline{\tilde{\omega}}_B - \underline{\omega}_{IB}^B \right) \tag{3.63}$$

Alternatively, a second order tracking law could be formed using estimated values for the derivatives of the rates:

$$\underline{m} = -K_5 \left(\underline{\tilde{\omega}}_B - \underline{\omega}_{IB}^B \right) - K_6 \, \underline{\dot{\omega}}_{IB}^B \tag{3.64}$$

Linear Control Law

The linear control law for the spacecraft equations based on the desired spacecraft rates above is simply (using either Equation 3.63 or 3.64)

$$\underline{\tau} = A^{-1} \, \underline{m} \tag{3.65}$$

The predicted response for this controller is found by substituting Equation 3.65 into the non-linear dynamic equation of motion, Equation 3.48.

Nonlinear Control Law Using Feedback Linearization

The control law which should compute the control torque inputs to the reaction wheels which provides the "desired" linear response governed by Equations 3.63 or 3.64 is Equation 3.49, which is repeated here for direct comparison with Equation 3.65:

$$\underline{\tau} = A^{-1} \left[-\underline{\omega}_B \times (J\underline{\omega}_B + \underline{h}) - A\underline{m} \right] \tag{3.66}$$

Figure 3-5 illustrates the overall spacecraft control strategy using feedback linearization and the estimated rates.
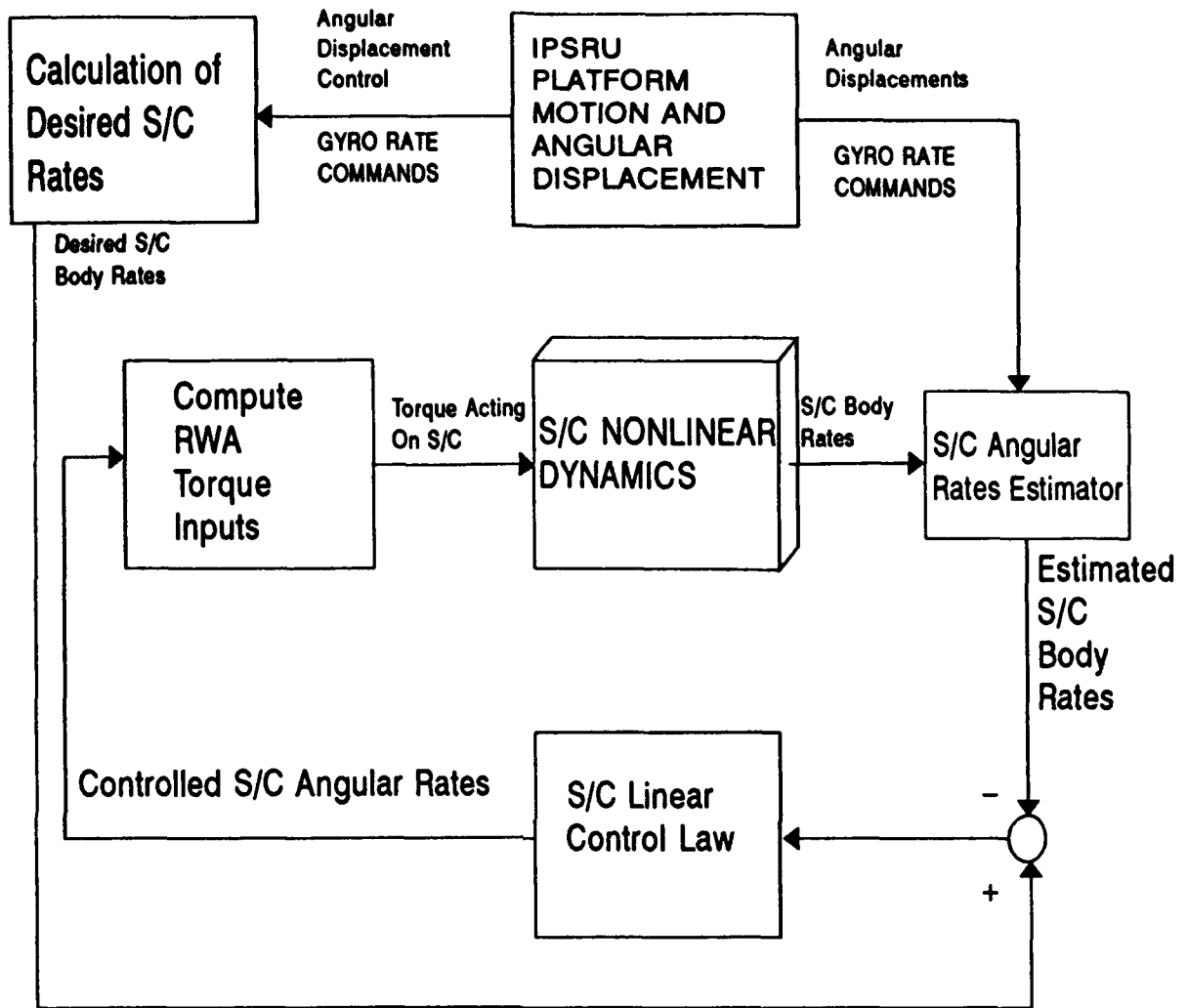
Figure 3-5: Spacecraft Controller Structure

Chapter 4

IPSRU Platform Control

The controller designs presented in Chapter 3 were based on many idealized assumptions for both the plant parameters (such as the inertia tensor) and the availability of measurements. The approach to designing the actual controllers used in this thesis was deterministic from the standpoint that they were designed under ideal assumptions, tested with various test cases for the uncertainties and then were tuned to increase performance. The "truth" models used for comparison with the nonlinear system simulations were the ideal linearized systems as shown in the previous chapter. This and the next chapter closely follow Chapter 3 in that the IPSRU platform control is developed first, followed by the spacecraft controller design for both the regulation of the angular displacement and the commanded rate tracker. Simulations illustrating comparison of the ideal linear system response with the nonlinear simulations under both ideal and uncertain conditions are presented. In addition, simulation issues are discussed to highlight the approach for future analysis and design of the attitude control system. The platform control is considered separately in this chapter and spacecraft controller design and the angular displacement regulator results are described in Chapter 5.

4.0.3 Controller Design and Simulation Procedure

The general design approach for control of the IPSRU platform and the spacecraft follow the same process:

1. Design the linear controller assuming exact linearization is accomplished.

2. Test the linear controller for expected performance under the assumption the exact linearization will cause the behavior of the nonlinear system to act as a "linear" system. This performance then becomes the truth model for desired performance.

3. Test the nonlinear controller using the linear control design against the same tests used for the linear system in step 2. If the controller structure is correct, the response should be the same as the linear system response.

4. Compare the performance to that of a linear controller used in the nonlinear system. This approach ignores the nonlinearities in the control design.

5. Test both the nonlinear and linear controllers against a perturbed plant model and under the influence of measurement noise.

6. Tune the controller based on simulation results. The feedback linearization technique allows the design of a linear controller in a structured manner, rather than by trial and error; however, as with any nonlinear system, some trial and error is expected.

This design approach is heavily dependent on the simulation, so every attempt was made to validate each segment of the simulation using combinations of analytical techniques and comparing the results with simulations using other techniques. For example, the spacecraft equations of motion were tested using closed form solutions for various rigid body cases which were compared to the same test case using the numerical integration technique outlined in Appendix E. Although the details of these types of tests are not included in the thesis, they will be described where appropriate to ensure reproducibility of the overall simulation.

The overall design was accomplished incrementally. The IPSRU platform controller was designed, simulated and tuned assuming knowledge of the z-axis gyro measurement. The spacecraft controller was then developed assuming the IPSRU rate commands were available. The two controllers were then integrated into one simulation, where the same test cases were run under the expectation that the results should be similar to the independent IPSRU platform and spacecraft controller simulations, as the coupling terms due to the angular displacement between them is required to be small. The linear truth model was used as both a benchmark and as a method of gaining intuition into the results of the nonlinear simulation.

The simulations are "continuous time" simulations as the controllers and computed parameters are integrated into the solution of the state equations for each simulation, contrasted with the approach which would compute the control inputs outside of the integration loop for the kinematic and dynamic state equations (essentially discrete-time control). This method was used as the development of the control problem formulation in Chapter 3 and the appendices was a continuous-time architecture; thus the controller designs were also accomplished using continuous-time design techniques.

4.0.4 Test Cases

The lengthy computation time (10-16 hours depending on the step size and whether the full simulation was used) limited the number of test cases which could be analyzed. Two of the more notable cases are shown here to illustrate the overall worst cases of several attempted. A "test case" is defined by the initial conditions; variations in the controller used for a simulation are subsets of each case. The cases were chosen based on the desire to illustrate the cross-coupling and nonlinear effects and also were designed to push the limits of controller performance from the start. The cases are detailed in Table 4.1. The cases are based on a 30 second slew to acquire a target which would be at the maximum target angular rate ($\omega_{Ti} = .025$ rad/sec) at the time of acquisition for a 555 km altitude [21]. The spacecraft and IPSRU rates are assumed to be equal at the start of the simulation, although there is some relative motion in effect between the platform and IPSRU through the angular displacements θ_x and θ_y and their rates, both of which are picked to be going in the "worst" direction opposite the desired target. The z-axis rate is assumed to be small but not zero. Case 1 corresponds to a slew of approximately 45 degrees where the x and y components of the unit vector are the same magnitude and their derivatives are moving in the opposite direction of the target unit vector; this case is useful for illustrating the computation of the IPSRU rate commands as they should be very close to each other. The second case is a single axis slew around the y axis of 73 degrees ($u_z = 0.3$), and is useful for illustrating the differences between the use of the linear and nonlinear controllers as the cross-coupling will be evident; additionally, the reaction wheels will be stressed for a single axis in order to perform such a large reorientation. The angular rate initial conditions ω_{P_x} and ω_{P_y} are not listed, but are computed at the beginning of each

64

simulation using Equations 3.31 and 3.32.

Table 4.1: Test Cases: Initial Conditions

State Variable	Case 1	Case 2
u_x	0.5	0.9539
u_y	-0.5	0
$\dot{u}_x$ rad/sec	0.02	0.02
$\dot{u}_y$ rad/sec	-0.02	0
θ_x (rad)	0.002	0.002
θ_y (rad)	-0.002	-0.002
$\dot{\theta}_x$ (rad/sec)	1.9e-4	1.9e-4
$\dot{\theta}_y$ (rad/sec)	2.1e-4	2.1e-4

The combinations of controllers which were simulated involve combinations of the linear and nonlinear controllers for each case. The nonlinear and linear IPSRU controllers were simulated separately, and then against the nonlinear and linear spacecraft controllers. This approach is intended to provide a direct performance comparison and will determine if the overall satellite control system architecture is feasible.

4.1 IPSRU Platform Controller Design and Simulation

Recall from Chapter 3 that the IPSRU controller was designed as the control of a free body, where the goal was to command the rate gyros to orient the IPSRU platform coordinate frame to line up its z-axis unit vector with the target unit vector coordinatized in the IPSRU frame, at which point the IPSRU reference beam LOS is pointed at the target. The platform is only controllable in two axes and is physically limited by the flexure hinge which joins the IPSRU platform to the spacecraft body. Several features of this approach are considered in the design of the controller:

1. The controller must command the platform such that the x and y components of the unit target vector go to zero, at which point the unit target vector direction is coincident with that of the IPSRU frame z-axis.

2. The angular rate around the z-axis is not controllable in this simulation, as the platform is only controllable in two axes. The third axis will be controlled by the spacecraft as developed in Chapter 5.

3. The unit target vector will have an angular rate whose calculation can be accomplished as shown in Appendix C (Equations C.33 or C.34). It is desirable to have the IPSRU coordinate frame rate match the target unit vector rate at the time of acquisition. This indirectly implies that control of the direction cosine components must include a method of controlling their rate as well as their magnitude.

4. The trajectory during the large angle slew is not explicitly controlled, but it is examined closely in the simulations because of the desire to limit the angular rate (which will translate to torque inputs to the reaction wheels) and acquire the target with the orientation and rate within the bounds required to operate the payload. Additionally, the magnitude of the slew is mathematically (not physically) limited by the restriction on the magnitude of u_z for the feedback linearization controller, which can avoided by retargeting through an intermediate trajectory [22]; in *practical* terms, this can easily be overcome by operational restrictions which appear to be acceptable as shown by the initial mission planning.

These considerations played heavily in picking the form of the linear controller design used for both the linear and nonlinear controllers. In addition to the fixed time controllers described in Chapter 3, constant gain linear feedback controllers were initially attempted because of their computational convenience and the hope they would perform adequately. They were not used in the end as high controller gains were needed to ensure that the target unit vector lined up with the IPSRU frame z-axis at the end of the slew; this resulted in unacceptably high rate commands. However, once the target is acquired they may be used for the tracking controller which tracks the target rates ω_{T_x} and ω_{T_y}.

The second type of linear controller approach considered was one which used a quadratic cost function which had penalties on the trajectory, control effort and final state. This approach was abandoned because it requires numerical integration of the Riccati equations and would significantly impact the complexity of the already complex nonlinear controller.

The finite-time proportional controller was then considered for its closed-form solution (Equation 3.12) and in fact did command the IPSRU platform to reach the desired target unit vector; however, the rate of change of the direction cosine components, $\dot{u}_x$ and $\dot{u}_y$, were not close to zero and as a result there would be difficulty in tracking the vector once it had been acquired. Thus the focus of the design turned to a second order finite-time controller, at the expense of having to estimate the derivatives of the direction cosine components (which was actually considered in the previous controllers as well), but with the advantage of the ability to affect the final states of both the direction cosine elements and their rates. Additionally, a closed form solution for the time-varying gains makes it more computationally feasible than the controller which penalizes both the final state and the trajectories of the states.

One other factor which should be noted is the length of time for the slew. The initial mission planning determined that a 60 second slew would be reasonable, which is very fast by most satellite standards (for up to a 70 degree reorientation). This was also picked based on the predicted maximum angular rates of the spacecraft which were in turn based on the size of the reaction wheels, as shown in Chapter 2. Two factors led to a more performance oriented 30 second slew time: first, the simulations were excessively long and the most interesting portions of the simulation turned out to be the transients at the early stages of the maneuver, and second, the spacecraft was re-sized to a lighter mass than the initial design which provided additional angular rate capacity. To the operationally oriented engineer there are two possible options for calculating the time-varying control gains. The first is to *always* fix the maneuver time interval as 30 seconds (or perhaps some other time), with the advantages of potentially storing precaculated time-varying gain vectors and also consistent mission planning constraints. The second is to calculate the gains on-line, which has the disadvantage of computation but allows for additional operational flexibility, and perhaps enhanced performance as longer time intervals require less active control, which may be beneficial in conserving the torque capacity of the reaction wheels. Under the latter scenario, for instance, the target vector uploaded to the vehicle may include a start and stop time which form the interval for calculating the gains.

4.1.1 Analysis and Results of the Second Order IPSRU Fixed Time Controller

The fixed time cont :oller used here was based on a cost functional that weighted the final state and the control effort as shown in Equation 3.22 in Chapter 3. As will be shown, this results in control gains that are minimal at first and then increase towards the end. Several "handles" used to tune the controller included the weights on the cost function, the various initial conditions for the target inertial rates and target unit vector coordinatized in the IPSRU frame and the actual time interval of interest. In all cases, extremely conservative numbers based on actual estimated rates were used to get a feel for the effects of these tuning parameters.

Stability analysis has not been developed here, although the foundation is laid by attempting to understand the physical bounds on the various parameters. The near perfect idealizations also need to be stretched in order to understand the robustness and real performance capabilities of the system. Physical plant parameters are and errors can be quantified but modeling dynamics errors and other non-parametric uncertainties must be looked at primarily from an analytic viewpoint. The results presented in this section are essentially empirical and provide a source of intuition for future analysis. The use of time varying gains preclude the use of frequency domain techniques, although the structure of the feedback (using convex cost functionals) is stabilizing in the deterministic ideal linear case as shown in many texts, such as [15] or [16].

Case 1 Results

Case 1 is an example of a large angle slew with initial conditions shown in Table 4.1. In addition, constant values (in rad/sec) $\omega_{Tx} = .025$, $\omega_{Ty} = .025$ and $\omega_{P_z} = .003$ are used. The particular control weightings used were determined by iteration, comparing the control gains to the errors at the final time. The scenario is a pre-target acquisition slew of 30 seconds, at which time the target would be acquired. The first example, Case 1, steps through the actual outputs of one complete software run for the IPSRU fixed-time second order controller. The simulations numerically integrated the state equations between intervals of 0.05 seconds, where the step size between each interval is determined adaptively by the MATLAB function ode45 with a tolerance of 1e-6.

Figure 4-1 is an example of the control gains which are solutions to the optimal control

problem of the linearized system. The gains used for the analysis were determined iteratively; the initial designs were attempted with higher penalties, which resulted in higher gains toward the end of the interval, and associated simulations resulted in high control activity. As a result the state penalties were lowered, with the following state weighting matrix used in the simulations:

$$S = \begin{bmatrix} 10 & 0 \\ 0 & 3 \end{bmatrix}$$

This penalty matrix weighs the states u_x and u_y more heavily than their derivatives. The same penalties were used for both the x and y axes since the this phase of the design does not include the needed detailed mission analysis necessary to determine the typical axes motions and cyclic torques (which may affect the reaction wheel sizing). Also, the inertia components are nearly equal for these axes so the rate commands calculated for the IPSRU portion should yield similar results in each axis for the spacecraft simulations. It also simplifies the calculations required for this analysis. The control gains were calculated using the analytic solutions to the Riccati equations as functions of time-to-go. Notice they start small and are somewhat level until the time-to-go gets smaller, where they peak. This is expected as the trajectory itself is not weighted, only the control effort and the final states. The magnitude, length, and sharpness of the hump are affected by the weightings. Because the controller is second order both u_i and $\dot{u}_i$ are controlled states, which indirectly affects to the IPSRU input rate commands.

The ideal linear control system was simulated by numerically integrating the closed loop state transition matrix from Chapter 3, Equation 3.30, and initial conditions for u_x, u_y, $\dot{u}_x$ and $\dot{u}_y$. The response plots are identical to the nonlinear simulation using the feedback linearized controller (for those states, as ω_{P_x} and ω_{P_y} are not calculated). Thus the nonlinear controller plots for these states in Figure 4-2 illustrate the results of this control law when applied to the linear system. The magnitude of u_z initially starts at approximately 0.7 (calculated from the initial conditions for u_x and u_y) and starts moving in the wrong direction—a result of the low control gains at the start combined with a "worst case" scenario where the initial direction cosine elements are already moving in the "wrong" direction. This highlights the need to monitor the magnitude of u_z as the cost function does not penalize the trajectory. The magnitude of u_z
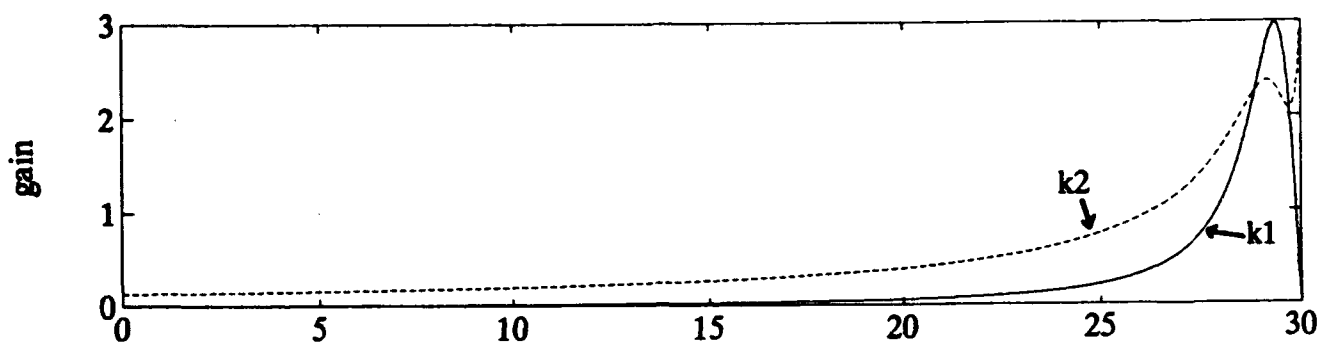
69

Figure 4-1: Typical Finite-Time Control Gains

reaches 1.0 at the acquisition ($t = 30$ sec) which means the target unit vector coordinatized in the IPSRU frame is pointed at the target. Figure 4-2 also shows the results for the other components of the unit target vector—both u_x and u_y to to zero which is the control goal as described above.

The simulation in Figure 4-2 is the nonlinear simulation for the feedback linearization controller and the linear controller as applied to the IPSRU kinematic equations. The nonlinear and coupled state equations were numerically integrated using the adaptive step size Runge-Kutta (MATLAB function ode45). The solution to the nonlinear set of differential state equations was computed between time increments to include the calculated results in the feedback loop. The plot includes the results for both the feedback linearized controller (solid line) and the controller calculated ignoring the nonlinearities (dashed line). This convention will hold for the remaining plots in this chapter unless otherwise noted. A comparison with the idealized linear system response shows the nonlinear controller achieves exact linearization as the plots are nearly identical.

Comparison of the results using the nonlinear controller with the linear controller does not show any dramatic increase in performance for this case. Both controllers command the platform such that the target unit vector lines up with the IPSRU platform z-axis, and both controllers command the platform rates to match the target rates.   nlinear controller
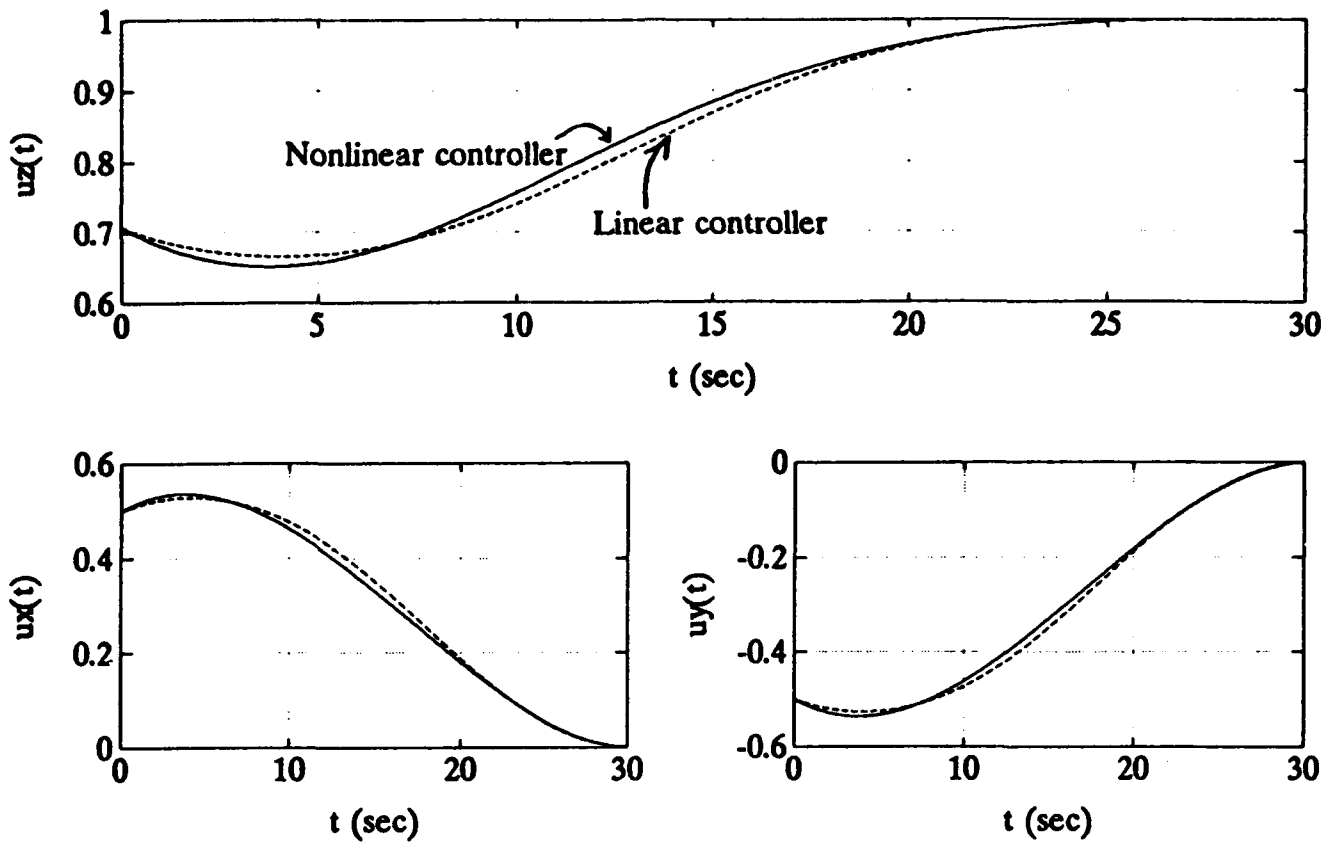
70

Figure 4-2: Case 1 IPSRU Platform Control Simulation

actually allows for a larger excursion of u_z. However, Figure 4-3 shows the nonlinear controller has lower peak rates which will result in l̶o̶w̶.̶ ̶ ̶w̶heel speeds for the spacecraft, which is advantageous as momentum management is alwa᷄ ᛫᛫ ᛫ssue with momentum exchange control systems. It is interesting to note both controllers appear to act the same towards the end as at that point the system enters the "linear" region—i.e. the z-axis is close to pointing at the target, the magnitudes of the x and y direction cosine elements are small, and examining the IPSRU kinematic equations (Equations 3.6 and 3.7) reveals a system which is evidently linearizable simply by ignoring the nonlinear terms as was done initially by the linear controller.

Table 4.2 lists the conditions of the states at the end of the simulation; the numbers listed are for a simulation of 0.05 second increments; the results do vary slightly when the step size is varied (the smaller the step size, the closer the system gets to the ideal linear case) and 0.05 was found to adequate for comparitive purposes. If the feedback linearization is truly

71

exact the ideal linear system would match the nonlinear controller system simulation results; both are numerically integrated and the magnitude of the results indicates probable numerical integration errors building up slightly in each case (perhaps due to the tolerance used for the Runge-Kutta routine). Additionally, the control gains were generated at 0.05 second increments and interpolated between the steps, which will induce some error (especially at towards the acquisition time as they are rapidly changing). The linear controller could be improved upon to place more emphasis on the final rate; the iterations to determine the final state penalty function weighting matrix showed the peak gains increase proportionally to the weight on that state without improving the inital gains very much. The numbers for the ideal linear system, linear controller, and nonlinear controller are all about the same magnitude and are acceptable, so overall the results of the simulations for Case 1 using the fixed-time controllers does not present a compelling reason to use the more complex nonlinear controller.
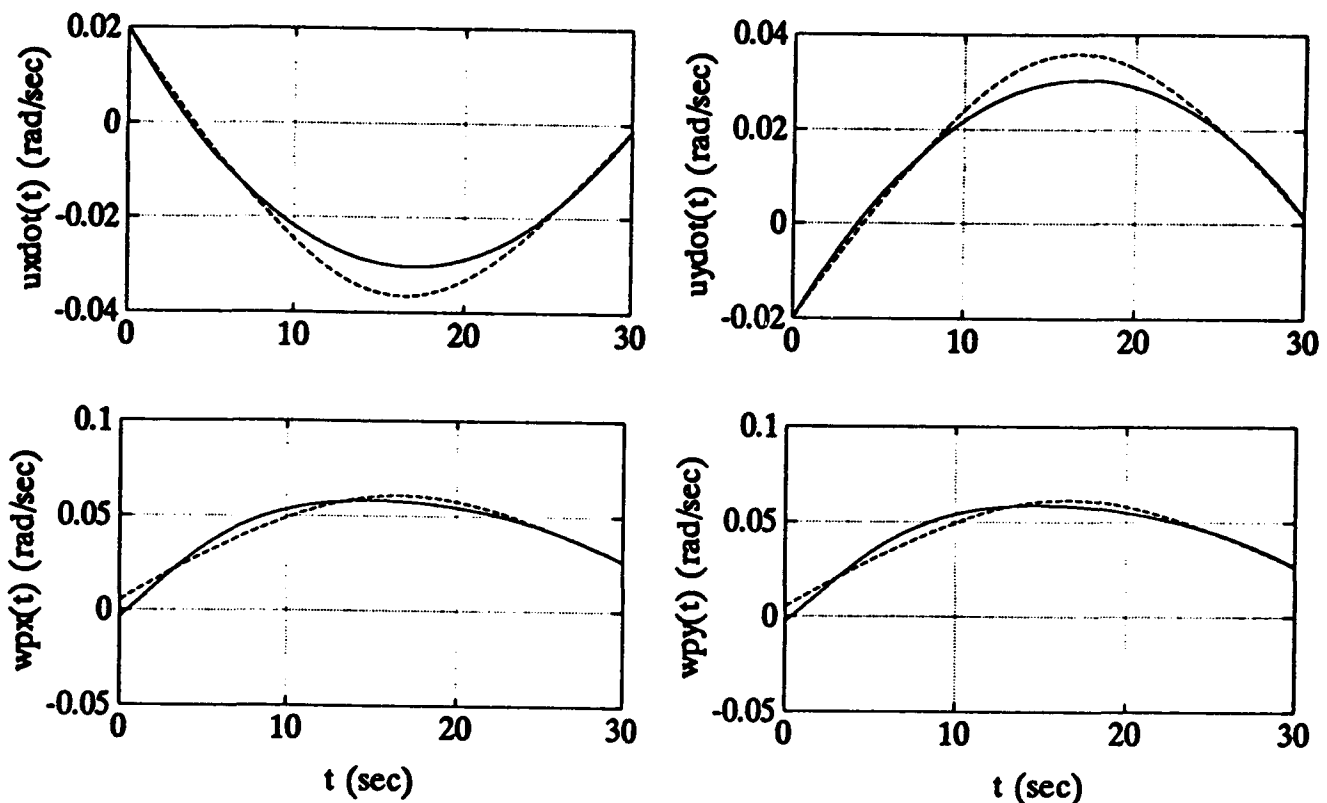
Figure 4-3: Case 1 Rates

72

Table 4.2: Case 1 Results for IPSRU Platform Control

PARAMETER	IDEAL LINEAR SYSTEM	LINEAR CONTROLLER	NONLINEAR CONTROLLER
u_x	3.4897e-5	5.1740e-5	7.7475e-5
u_y	-3.4897e-5	-5.8251e-5	-7.7475e-5
u_z	9.9999e-1	9.9999e-1	9.9999e-1
Pointing Error (deg)	2.8277e-3	4.4640e-3	6.2777e-3
$\dot{u}_x$ (rad/sec)	-1.4851e-3	-1.3424e-3	-1.48567e-3
$\dot{u}_y$ (rad/sec)	1.4851e-3	-1.3639e-3	1.4856e-3
ω_{P_x} (rad/sec)	2.6485e-2	2.6364e-2	2.6236e-2
ω_{P_y} (rad/sec)	2.6485e-2	2.6342e-2	2.6736e-2
Rate Command Error (rad/sec)			
$\omega_{P_x} - \omega_{T_x}$	1.4850e-3	1.3636e-3	1.2357e-3
$\omega_{P_y} - \omega_{T_y}$	1.4852e-3	1.3424e-3	1.7357e-3

Case 1 establishes the feasibility of using this type of controller for large angular reorientations. The initial conditions on $\dot{u}_x$ and $\dot{u}_y$ were chosen to "push" u_x and u_y to larger values, which would create problems in the nonlinear control of the unit vector as u_z would get close to one. The next case illustrates a single axis slew of about 73 degrees, which is the maximum expected slew for this mission.

Case 2 Results

The plots in Figures 4-4 and 4-5 illustrate the differences between the linear and nonlinear controllers, especially in the cross-axis coupling. The plot of u_z shows its magnitude getting near zero early on, as the initial slew angle is larger and the initial conditions for the direction cosines the "wrong direction" in terms of rate, or the target vector as seen by the IPSRU platform is moving away from the IPSRU z-axis unit vector. The IPSRU commanded rates are shown for comparison with the last case; note the larger maximum direction cosine element rates which appears to be due to the controller attempting to control the larger excursion of u_z.

This case is more dramatic in showing the effects of the nonlinearities and cross coupling in the kinematics of the target vector in the platform frame. The results in Figure 4-4 show the nonlinear controller slews only about the desired axis, while the linear controller exhibits cross-
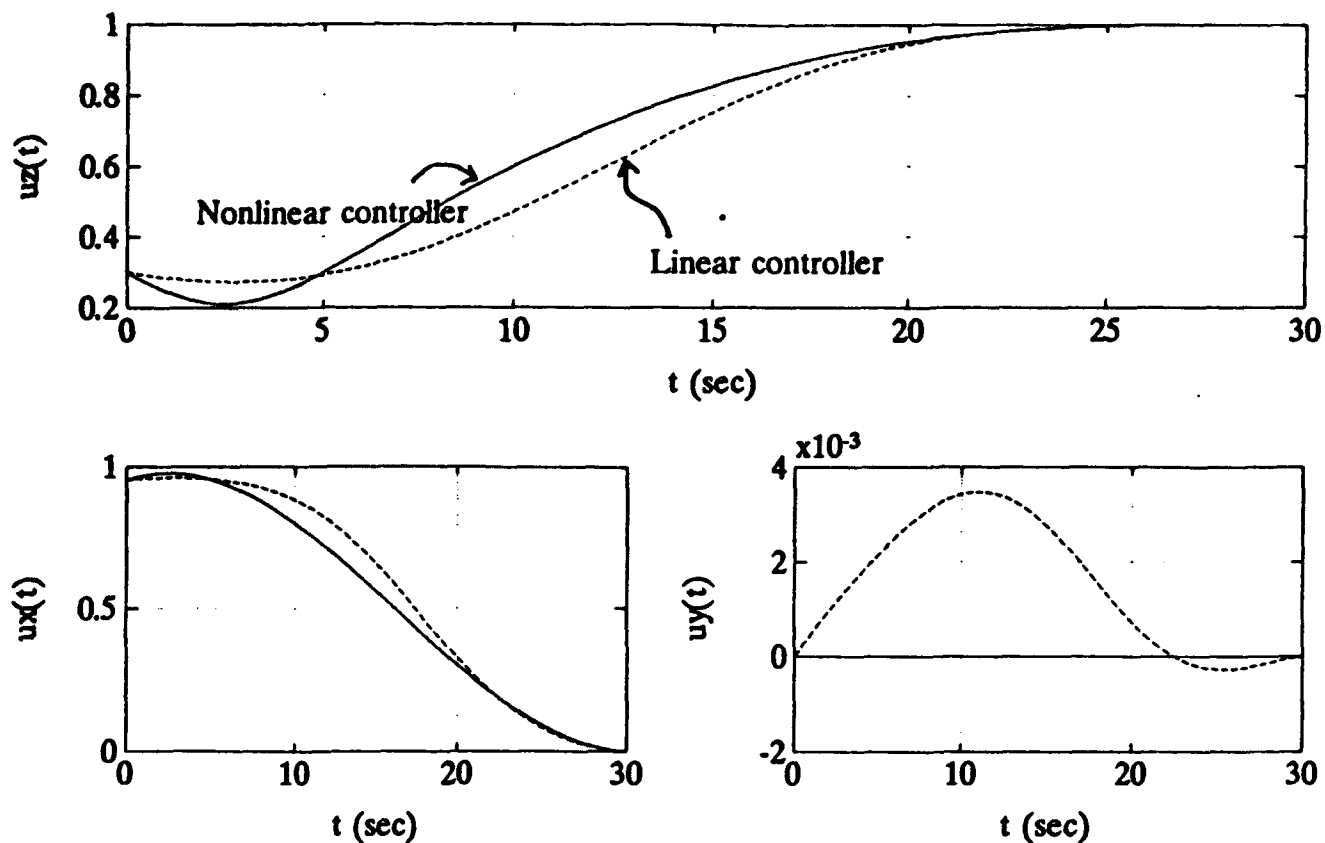
73

Figure 4-4: Case 2 IPSRU Platform Control Simulation

coupling as the term u_y does not stay at or near zero, and thus additional rate commanding is needed to control the cross coupling in the coupled axis. Both show again the need to monitor the magnitude of u_z as it dips lower than the arbitrarily set limit of 0.3; this dip is attributable to the very small rise in magnitude in u_x which is a result of the finite controller gains.

The linear controller response matches the ideal linear system response; however, the linear controller actually appears to provide smoother command inputs and actually has less error in achieving the target rate command at the acquisition time (although it may be due to the numerical integration as mentioned in the previous case). This may be attributable to the nonlinear controller not only achieving linearization as a function of u_z, but also for the compensation for cross coupling in the z-axis through the term ω_z. If this explanation is correct, this term will show up in the spacecraft simulation. The rate of change of the direction cosine components is lower for the nonlinear controller, indicating that energy is conserved
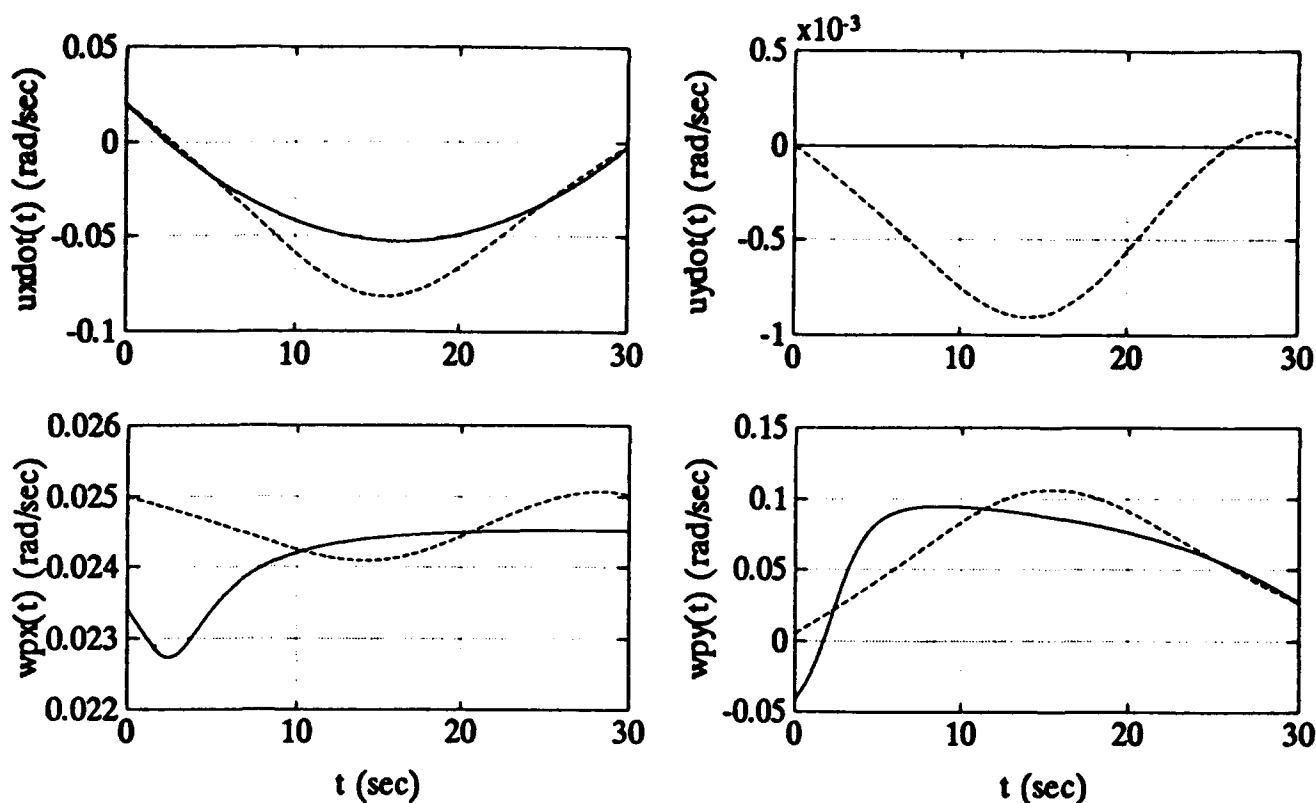
Figure 4-5: Case 2 Rates

in terms of the idealized linear system parameters, which may end up translating to lower wheel speeds in the full spacecraft simulation for the nonlinear controller as compared to the linear controller. However, this acquisition results for this case demonstrate there may not a be significant performance advantage to using the more complicated nonlinear controller. This is attributable result of placing the control goals in terms of the direction cosine component magnitudes and rates, which only indirectly affect the commanded rates to the IPSRU platform (recall the linear controller attempts to control the target vector direction cosine elements by the platform rate commands). Additionally, the nonlinear controller does perform to the level of the ideal linear control simulation for those state variables. It may just be fortuitous that the linear simulation achieved better performance in some areas, which could only be verified by simulating a much larger set of test cases. The results for the simulation end points are listed in Table 4.3.

Table 4.3: Case 2 Results for IPSRU Platform Control

PARAMETER	LINEAR CONTROLLER	NONLINEAR CONTROLLER
u_x	3.3454e-5	1.253e-4
u_y	-5.9103e-6	-2.5000e-20
u_z	9.9999e-1	9.9999e-1
Pointing Error (deg)	1.9464e-3	7.1802e-3
$\dot{u}_x$ (rad/sec)	-1.8450e-3	-2.4503e-3
$\dot{u}_y$ (rad/sec)	2.3918e-5	6.4147e-20
ω_{P_x} (rad/sec)	2.5024e-2	2.4523e-2
ω_{P_y} (rad/sec)	2.6845e-2	2.7450e-2
Rate Command Error (rad/sec) $\omega_{P_x} - \omega_{T_x}$ $\omega_{P_y} - \omega_{T_y}$	2.3918e-5 1.8449e-3	-4.7695e-4 2.4503e-3

4.2 Platform Control Simulation Results

The overall results indicate that there may not be any performance advantage to using the nonlinear controller in terms of the performance goal of acquiring the target vector at the target rate. Both controllers provide the desired attitude accuracy, especially considering the size of the angular reorientation. The nonlinear controller does in fact appear to produce a linear input/output relationship which aids in controller design—the initial nonlinear simulations for the nonlinear controller could be accomplished with a linear system model, which would be much faster and easier to construct. The success of the linear controller on achieving the desired performance warrants consideration from the standpoint of simplicity and implementation in the overall spacecraft control structure. However, the linear controller shows a tendency for higher rates, especially for the single axis slew, which is a serious consideration for a spacecraft which needs to minimize angular momentum buildup in any axis in order to minimize the need for wheel desaturation maneuvers. The overall spacecraft simulation is needed to verify the expectation that the linear controller will translate into higher reaction wheel activity, which may or may not be acceptable. Additionally, control of the z-axis may be affected by the use of the linear controller as compared to the exact linearization controller which compensates for the rate.

The choice of the cost function which only penalized the final states of the direction cosine

components and the control effort (a linear function of the direction cosine component rates) appears to be acceptable in terms of gaining the desired endpoints; however, the addition of penalty along the trajectory may be considered to attempt to control the rate of change of the unit target vector direction cosine components. Other cost functions may be used as well, perhaps even nonlinear convex cost functions which directly address the problem of penalizing the angular rate input commands' trajectories and endpoints. The overall controller structure performance cannot be fully ascertained, however, until it is integrated into the complete control system, which is accomplished in the next chapter.

Chapter 5

Spacecraft Control

The control system architecture for this satellite requires the spacecraft to "follow" the IPSRU platform rate commands while keeping the angular displacement between the platform and spacecraft body near null. The spacecraft is controlled by reaction wheels which exert a torque on the spacecraft body by responding to command inputs which cause the wheel speeds to change, resulting in an adjustment of the orientation of the overall spacecraft angular momentum vector. The platform kinematics will cause the angular displacement between the platform and the spacecraft to change, so a method of regulating this angular displacement is needed. This chapter presents the designs of the spacecraft control and angular displacement regulator, and presents the results of simulations which highlight the effects of using the nonlinear controller versus a linear controller. Additionally, simulations of effects of inertia tensor uncertainty and measurement noise are presented to demonstrate additional performance gains realized by the use of nonlinear controllers. The test cases used for illustration of the control system are the same as those in Chapter 4 from Table 4.1. The basic controller designs and simulations are presented first, followed by a look at the effects of inertial tensor uncertainty and measurement noise.

5.1 Spacecraft Control Design and Simulation

The basic goal of the overall spacecraft control design is to follow a desired rate command by computing a torque command input to the reaction wheel assembly. The rate command

has several components using the architecture developed in Chapters 2 and 3 (Figures 3-4 and 3-5): the IPSRU platform commanded rate coordinatized into the spacecraft body frame, the feedforward command used to anticipate the IPSRU platform motion and regulate its displacement, and the feedback command used to counteract the effects of disturbances. Features of this approach which warrant consideration include:

1. The reaction wheel speeds must be measurable.

2. The principal component of the angular rate commands to the spacecraft, the IPSRU platform rates coordinatized in the spacecraft body-fixed frame, are not directly penalized in the fixed-time IPSRU controller cost functional. They will, however, directly affect the reaction wheel speeds; the simulations will indicate the effects of the IPSRU control designs on the wheel speeds.

3. The sensors which measure the angular displacement between the platform and the spacecraft are extremely accurate high bandwidth sensors, and are assumed to measure the two-axis flexure hinge displacement under the assumption there is no misalignment or twisting of the platform.

4. The optical payload would not be operating during a slew to acquire a target but would operate (slew) when a target is tracked from the moving spacecraft, so it is always desirable to keep the angular displacement between the platform and spacecraft small to prevent hitting the flexure hinge stops and also to prevent saturating the input rate commands to the platform gyros. Note it may be simpler to clamp the angular displacement while slewing; this would require unclamping at the target with undesirable transients as there will always be a slewing between the spacecraft and target due to their relative motion. This also requires additional logic to change the attitude determination method to use the gyros in a strapdown mode which is undesirable. Therefore the approach assumes IPSRU as a free body with the spacecraft controlling the angular displacement by measuring the angular displacement and computing torque commands to the reaction wheels to regulate the displacement.

5. The stable platform only controls the inertial rates about two axes; the second gyro mounted to the platform of IPSRU controls the third as the spacecraft must be controlled

79

in three axes. The third axis gyro is mounted at the base of IPSRU and operates in a strapdown rate mode.

These features are considered in the design of the spacecraft controllers. The basic linear controllers (for the linearized system) for both the spacecraft and angular displacement regulator were designed using constant gains. This allows for some frequency response interpretation, but in the overall context of this thesis the real issues are the time domain effects of achieving the target accurately and avoiding excessive control activity in the reaction wheels and angular displacement.

The design of the simulation and the controller designs were developed incrementally. The first step was to program the spacecraft dynamic equations, verify them, and then design an exact linearization controller which was verified against an ideal linear model (similar to the IPSRU platform procedure). The controller design is based on the decoupled linearized model from Chapter 3:

$$\dot{\omega}_{Bx} = m_x$$
$$\dot{\omega}_{By} = m_y \quad\quad\quad (5.1)$$
$$\dot{\omega}_{Bz} = m_z$$

where

$\dot{\omega}_{B_i}$ represent the ideal linear system state equations under the assumption that the computed torque to the reaction wheels achieves and exact linearization of the input/output response in terms of the angular rates of the spacecraft with respect to inertial space coordinatized in the spacecraft body-fixed frame.

m_i are the torque commands which control the system to achieve the desired response for the idealized linear system.

Recall that in Chapter 3 a simple proportional tracker would be of the form

$$\underline{m} = -K_5 \left(\underline{\tilde{\omega}}_B - \underline{\hat{\omega}}_{IB}^B \right) \quad\quad\quad (5.2)$$

80

where

$\tilde{\underline{\omega}}_B$ is the desired angular rate of the spacecraft. Recall from Chapter 3, Equations 3.59–3.61, that the desired angular rates are computed using the IPSRU platform rates coordinatized in the s/c frame and the rate commands which regulate the angular displacement based on the platform motion relative to the spacecraft.

$\hat{\underline{\omega}}_{IB}^B$ is the spacecraft angular rate vector estimate which is based on the IPSRU platform angular rate commands, the platform kinematics relative to the spacecraft, and the spacecraft z-axis gyro data (from Equation 3.62).

The closed loop system based on such a controller responds essentially as a low-pass filter which is driven by the error signal between the desired spacecraft rate and the estimated angular rate. A higher order tracker could be developed using an estimate of the derivative of the spacecraft angular rates, resulting in a closed loop system which has a second order response (i.e. spring/mass/damper type of response) for controlling the error signal. Both controllers should drive the error between the desired rate and the spacecraft rate asymptotically to zero assuming that the poles of the closed loop system are chosen correctly (i.e. in the left-half of the $s-$plane). The bandwidth of the reaction wheels and spacecraft response is expected to be about 0.5 Hz, so the initial designs used controllers whose frequency response matched the expected bandwidth. The transfer functions for each controller could then be designed using pole-placement to match desired responses. The linear simulations were first accomplished using standard impulse and step responses, and it appeared that the second order controller had advantages in tracking error, transient performance and disturbance rejection. The controllers then were commanded to follow an input vector which was the output of the IPSRU platform simulation commanded rates; it became apparent that the first order controller was much easier to tune in terms of the x and y axis control responses although both controllers performed adequately in asymptotically driving the tracking error to zero without a lot of control activity. This can be accomplished by low gain designs, which result in an expected advantage of attenuation of high frequency noise; this is, of course, offset by decreased attenuation of low frequency disturbances.

The complete, integrated spacecraft model was then developed. The initial simulations used the same test cases as for the IPSRU platform and the initial spacecraft controller design. The

81

the angular displacement was then forced to zero (e.g. simulation of the platform rigidly fixed to the spacecraft) and verified against the results of the linear simulation for the spacecraft; the spacecraft rates followed the IPSRU commanded rates to match the cases for the linear system simulation which in turn indicated the feedback linearization was programmed correctly. The initial simulations were accomplished for a preliminary spacecraft configuration; the wheel speeds indicated that either the spacecraft inertias in the x and y axes were too large or the chosen reaction wheels were not capable of achieving the desired slew rates and would saturate. The spacecraft was resized and these simulations were rerun using the same reaction wheels. The "lighter" inertias resulted in more significant transient responses and the controllers had to be retuned. This is just one example of how the control design and spacecraft design are interrelated.

At this point the angular displacement regulator was designed. Again, the design was accomplished using linear techniques; the intended goal was to keep the regulation "tight" so that the displacement would not exceed 10 mrad. Thus the feedforward command included terms which anticipate the platform motion based on the estimated spacecraft rates and the angular displacement measurements, as developed in Chapter 3 and Appendix D. The design initially attempted was a controller based on a second order system closed-loop system response with a damping ratio of 1.0 and a natural frequency of π rad/sec. The first test cases included the same scenario as used before where the angular displacement was initialized at zero, only this time the platform was free to move based on its kinematics. The result was additional transient effects on the tracking of the IPSRU rates; additionally, after trying several combinations of control gains for the spacecraft and the angular displacement regulator it became apparent that the desired rate command to the spacecraft controller had to be slow enough so the spacecraft could follow the motion, or else transient performance became an issue. Additionally, the first order spacecraft controller was chosen for the x and y ease of tuning and adequate performance; it also does not require estimation of the spacecraft angular accelerations. Thus there is a tradeoff between the desire to tightly control the angular displacement while trying to minimize excessive reaction wheel activity due to the transients in the commanded rates. The z-axis control was accomplished by regulating the s/c z-axis to zero; assuming the angular displacements are regulated the actual IPSRU platform z-axis will go to zero as shown in

Equation 3.38. It is interesting to note that the performance of the IPSRU platform matched the free-body simulations of the previous chapter more closely than expected, except in a few controller designs where the angular displacement grew too large resulting in some minor cross-coupling feedback through the z-axis rate (which could not actually happen due to the limits of the flexure hinges). The remainder of the simulations indicate that the performance of the IPSRU platform control can be considered essentially independent of the spacecraft (under ideal modeling and measurements) as long as the angular displacement is small. This again points to the need for the wheel speeds to be monitored closely as the spacecraft must be capable of not only following the IPSRU platform rate but the more active feedforward commands from the angular displacement regulator. Figure 5-1 illustrates the basic simulation parameters for a Case 1 simulation using the nonlinear controllers; note the angular rate commands are nearly identical to the same case rate commands for the same case from Chapter 4 (Figure 4-2), with the exception of the initial transients.

The transient control issue became even more apparent in the final set of simulations using the ideal spacecraft model. Case 1 and Case 2 were tested; both of these cases stress the controller as they have initial components of angular displacement and rates, and the result was very apparent in the "start up" transient performance. The controller gains were again redesigned, and the critical factor for controlling the initial transients once again appeared to be the angular displacement regulator. The damping ratio was increased while the natural frequency was decreased, resulting in the displacement taking longer to settle to near zero with improvements in the wheel speed activity. Also, the z-axis control of the rate was changed to more tightly regulate the z-axis rate to zero; thus the final spacecraft controller structure was modified to include control of the angular acceleration. The final linear controller structure for the spacecraft and angular displacement regulator is shown in Figure 5-2 with gains listed in Table 5.1.

$$m_x = -k_7 \left(\tilde{\omega}_{B_x} - \hat{\omega}_{B_x} \right) \tag{5.3}$$

$$m_y = -k_7 \left(\tilde{\omega}_{B_y} - \hat{\omega}_{B_y} \right) \tag{5.4}$$

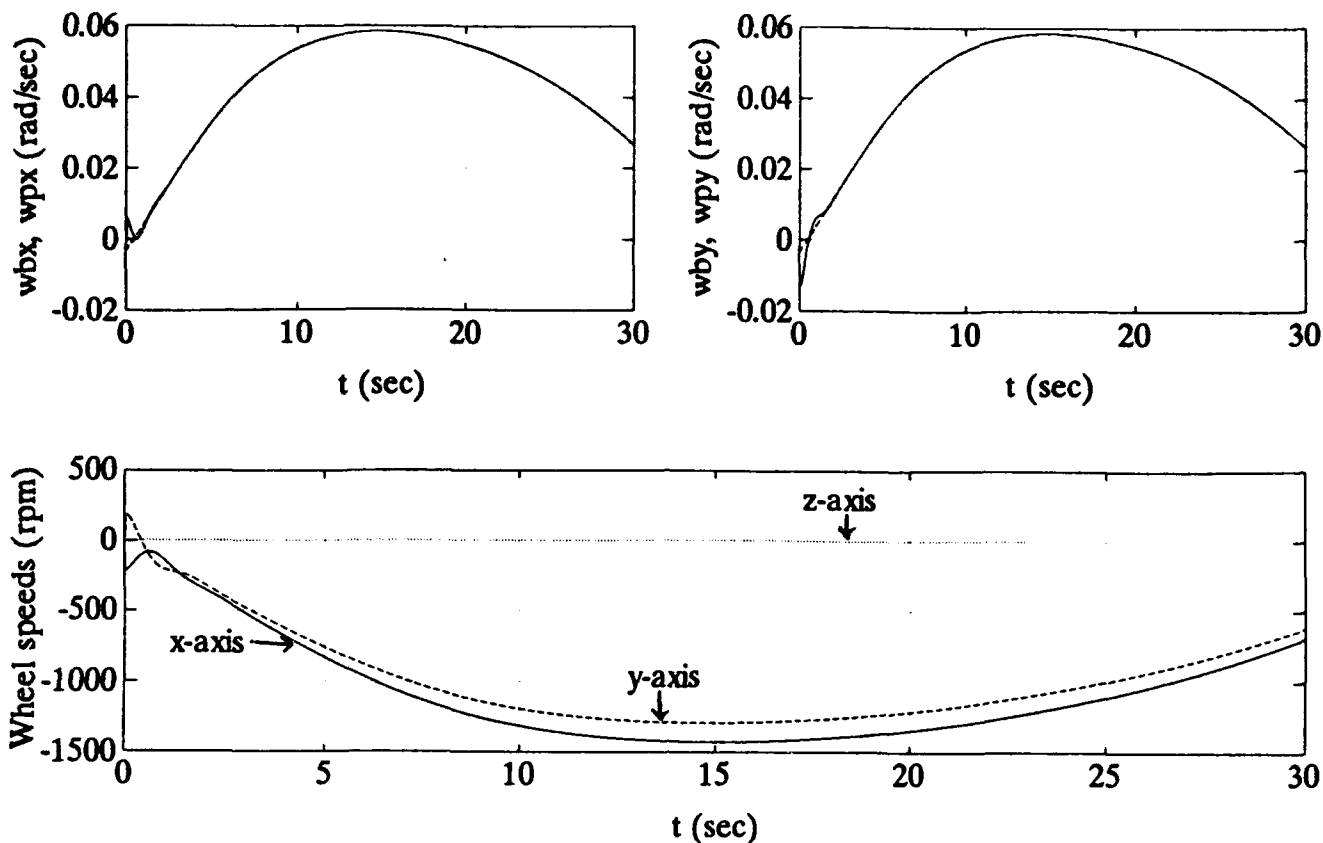$$m_z = -k_5 \left(\tilde{\omega}_{B_z} - \hat{\omega}_{B_z} \right) - k_6 \dot{\tilde{\omega}}_{B_z} \tag{5.5}$$

Figure 5-1: Case 1 Simulation Using Ideal Model and Nonlinear Controller

$$q_x = -k_3\theta_x - k_4\dot{\theta}_x \tag{5.6}$$

$$q_y = -k_3\theta_y - k_4\dot{\theta}_y \tag{5.7}$$

Table 5.1: Spacecraft and Angular Displacement Controller Gains

	K_3	K_4	K_5	K_6	K_7
Gain	3.1623	4.0404	16.0	5.6	4.5

The nonlinear controller is then computed using Equation 3.49 where the desired rates (including the IPSRU platform rate command and the angular displacement feedforward) are computed using Equations 3.59–3.61.
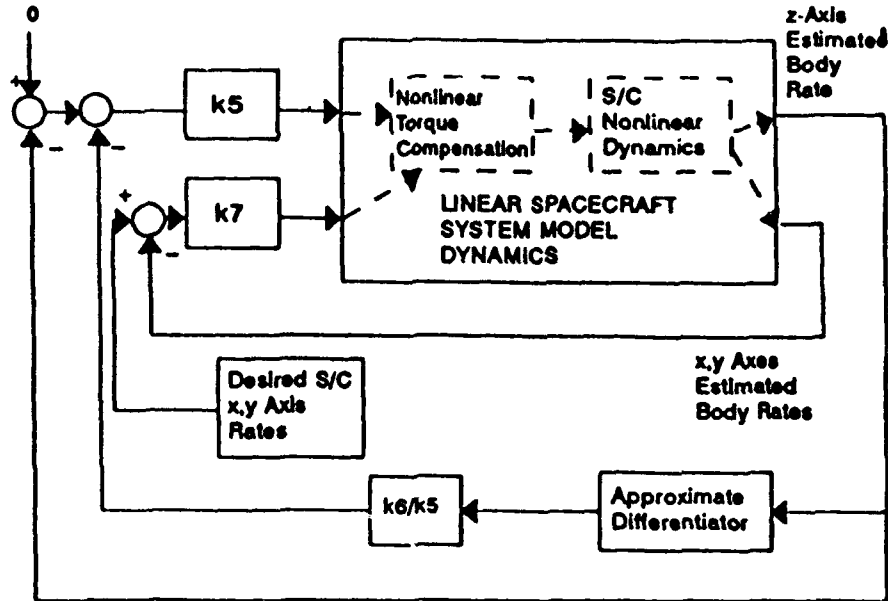
84

Figure 5-2: Spacecraft Ideal Linear Model Controller Structure

All of the final simulations where run using an interval step size of 0.02 seconds for 30 second intervals for comparative purposes. The tolerance for the MATLAB adaptive step size Runge-Kutta numerical integration error for all states was 1e-6. Thus, as with the IPSRU control simulations, some numerical error is likely to occur but the simulations should show the comparitive effects due to the actual structure of the controllers. Most of the plots are for a single run, in which case the solid line represents the x axis component, the dashed line represents the y component, and a dotted line represents the z component (unless otherwise noted). Finally, all of the rates plotted throughout this chapter are coordinatized in the spacecraft body-fixed frame in order to make meaningful comparisons.

5.1.1 Comparison of Linear and Nonlinear Controllers for the Ideal Model

The IPSRU platform simulations indicated that a linear controller may perform just as well as the nonlinear controller for target acquisition, with the supposition that higher wheel speeds would result. Both Case 1 and Case 2 were simulated using combinations of linear and nonlinear controllers. The results were as expected; the peak wheel speeds were larger for when the IPSRU

85

platform linear controller was used; in some cases as much as 200 rpm higher which could be significant in the overall operation of a satellite.

The IPSRU linear controller also resulted in higher overshoots in the angular displacement regulator which were within acceptable limits. The Case 1 results were not dramatically different in any other critical respects; however, the Case 2 results in Figure 5-3 show much more activity for the reaction wheels, especially in the cross-coupling and peak wheel speeds. This indicates that the nonlinear controller warrants additional investigation over a greater variety of initial conditions.
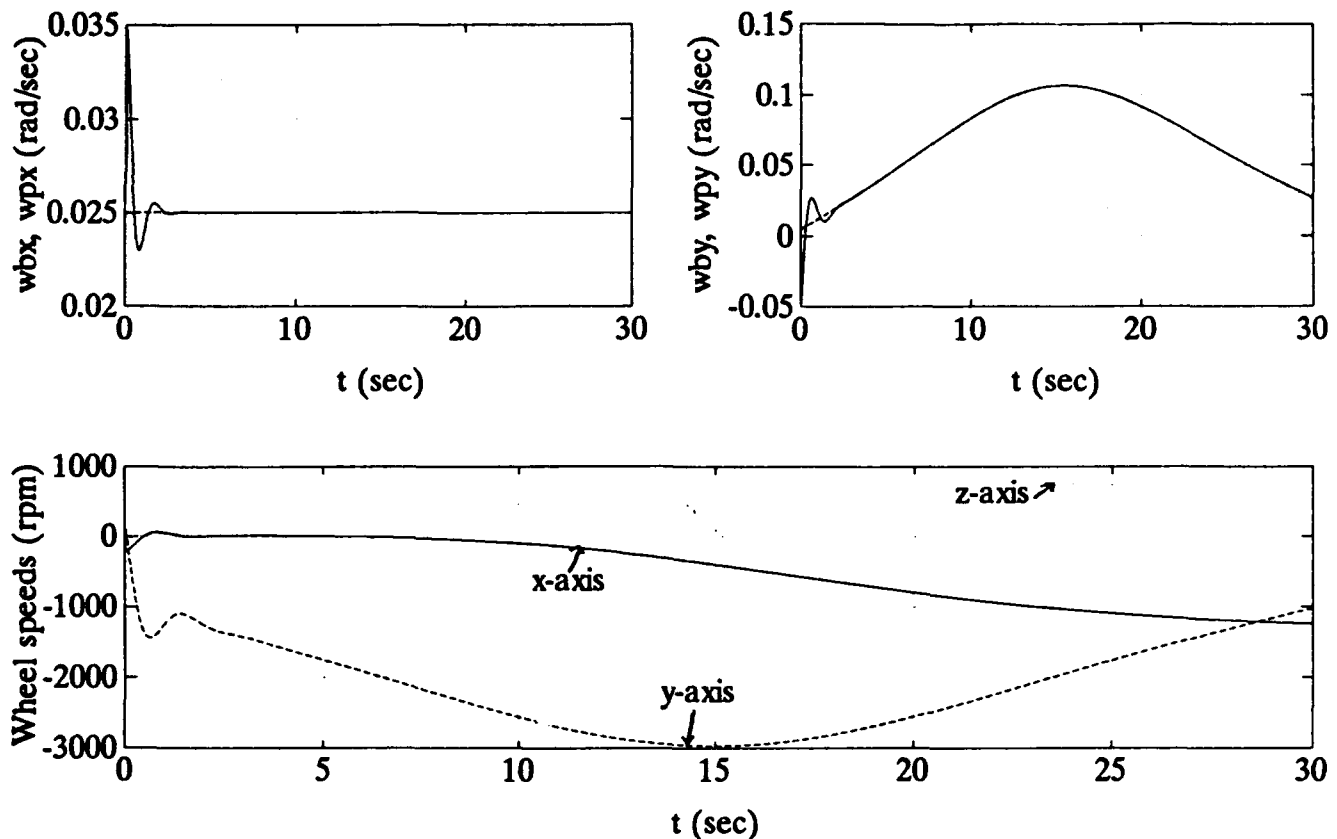

Figure 5-3: Case 2 Simulation Illustrating Effects of Nonlinear and Cross Coupling Terms

5.1.2 Disturbance Effects on the Ideal Model

The disturbances described in Chapter 2 have different effects on the spacecraft, depending on many factors such as the orbit and orientation of the vehicle. This simulation does not integrate

the spacecraft motion relative to the earth so a simple approximation is necessary to provide insight in to the effects of such disturbances. The effects of all the disturbances are lumped into one disturbance whose magnitude is equal to the sum of all the disturbances. This is then treated as a step input (e.g. a persistent disturbance) to the spacecraft equations of motion, where τ_d is the disturbance torque:

$$\underline{\dot{\omega}}_B = A^{-1} \left[-\underline{\omega}_B \times (J\underline{\omega}_B + \underline{h}) - \underline{\tau} + \underline{\tau}_d \right] \tag{5.8}$$

The magnitude of the step is assumed to be 5.0e-4 N $\cdot$ m $\cdot$ s in the pitch axis, as the gravity-gradient effects are generally along the velocity vector and under a nominal situation in nadir pointing mode the pitch axis will see this disturbance [14]. Additionally by only examining one axis the effects on cross coupling become apparent as a torque along the pitch x axis will result in an attempted precession of the y axis, which itself then will be counteracted by wheel speed changes in the x axis. Thus the wheels need to be sized to absorb the buildup of the angular momentum. Assuming the exact linearization for the system is accomplished by nonlinear feedback, the angular rate imparted to the vehicle is attenuated by the inverse of the controller gain in Equation 5.1 and Table 5.1. The angular rate which must be compensated based on these equations is then found by scaling the torque by the inverse of the pitch axis inertia, resulting in a step rate of approximately 1e-6 rad/sec (which is much smaller than the IPSRU platform control rates). The angular momentum storage (e.g. excess wheel speed capacity needed) is then found from the angular momentum, Equation 3.45 which is integrated over an orbital period to determine the wheel speeds in each axis. The original sizing in [26] accounts for this effect; this effect was not simulated due to computational limitations and requires additional simulation and analysis. This approximation is very conservative as the dominant gravity gradient torque will be cyclic over the orbital period due to the approximately oblate Earth geopotential model and therefore that component should average approximately to zero [14]. The effects of the other torques (aerodynamic, etc.) cannot be fully assessed without a complete orbital simulation, taking into account the actual mission and expected vehicle orientations throughout typical mission scenarios. Finally, the buildup of angular momentum must be occasionally counteracted by some sort of external opposing torque; the spacecraft design is capable of using either magnetic torquers or thruster firings to spin the wheels down

[26].

5.2 Effects of Inertia Tensor Uncertainty

The spacecraft inertia tensor is initially well known (at the time of launch) by careful manufac-
turing bookkeeping. However, as the vehicle ages and fuel is expended, there is no method of
actually calculating the distribution of the fuel accurately (although keeping track of thruster
firing times and/or pressure of the fuel tanks may provide a fairly good estimate) and the ef-
fects of manufacturing errors may be magnified. Thus there is an interest in how the controller
behaves in light of some uncertainty. Although the assumption in Chapter 2 that the spacecraft
inertia tensor is such that the mass distribution lies symmetrically along the geometric axes,
the control problem formulation in Chapter 3 does allow for off-axis inertia components in the
ideal model; this is in contrast with many attitude control schemes which rely heavily on this
assumption [13]. The simulation of the effects of the inertia tensor is accomplished by using a
perturbed plant model in the spacecraft equation of motion; this is accomplished by forming
a symmetric error matrix consisting of off-axis products of inertia and adding it to the truth
model inertia tensor:

$$J_{true} = J + J_{error} \tag{5.9}$$

To approximate a 10 percent uncertainty in the inertia tensor, the following error tensor was
formed simply by averaging the principal moments of inertia for each product of inertia and
multiplying by 10 percent, with small variations in the principal axes as well. For instance the
following expression was used for the simulation of Figure 5-4.

$$J_{true} = \begin{bmatrix} 99.2 & 0 & 0 \\ 0 & 89.8 & 0 \\ 0 & 0 & 147.6 \end{bmatrix} + \begin{bmatrix} .08 & -10 & -13 \\ -10 & 1.02 & -12 \\ -13 & -12 & -7.6 \end{bmatrix}$$

$$= \begin{bmatrix} 100 & -10 & -13 \\ -10 & 91 & -12 \\ -13 & -12 & 140 \end{bmatrix} \text{kg} \cdot \text{m}^2$$

Both test cases were tested using both positive and negative variations of 10% for both the linear and nonlinear spacecraft controller structures. The effect of the inertia tensor uncertainty is basically a disturbance torque to the spacecraft. The nonlinear spacecraft controller showed very little variation from the ideal model results in controlling the desired angular rates other than very small increases in the transient tracking error, wheel speeds (especially the z axis) and angular displacement regulation. The nonlinear controller has the advantage of canceling out a large portion of the inertia tensor variation assuming the true inertia is reasonably close to the model inertia tensor. The linear spacecraft controller simulation in Figure 5-4 shows larger transients in both the spacecraft rate and angular displacement , markedly increased wheel speeds in the z-axis and (not shown) a much larger angular rate around the z-axis. The system does eventually track the IPSRU command rates, however; this is an indication of the overall stability of the system in terms of rate.

The benefits of the nonlinear spacecraft controller became apparent very quickly for the uncertain inertia case; the specifications were met using the nonlinear IPSRU platform controller for both cases. However, when the linear platform controller was used with the nonlinear spacecraft controller, the transients were very high. In both cases the maximum angular displacement was at least 40% higher than the same case using a nonlinear platform controller (actually over three times higher for Case 2 y-axis). Figure 5-5 shows the angular displacement plot for Case 2 using this combination of controllers, and there is a very high overshoot in the y-axis which comes close to the angular displacement limit of 10e-3 radians.

Combining the linear spacecraft controller with the linear IPSRU platform controller was not simulated, but it is apparent that the result most likely would be significant in terms of the increased wheel speeds in off-axes and high angular displacement transients. Additionally, transients would take longer to die out, so disturbances acting on the spacecraft and initial conditions would have a more lasting effect. Overall, these simulations point to a different conclusion than the previous chapter: the nonlinear IPSRU platform controller in combina-
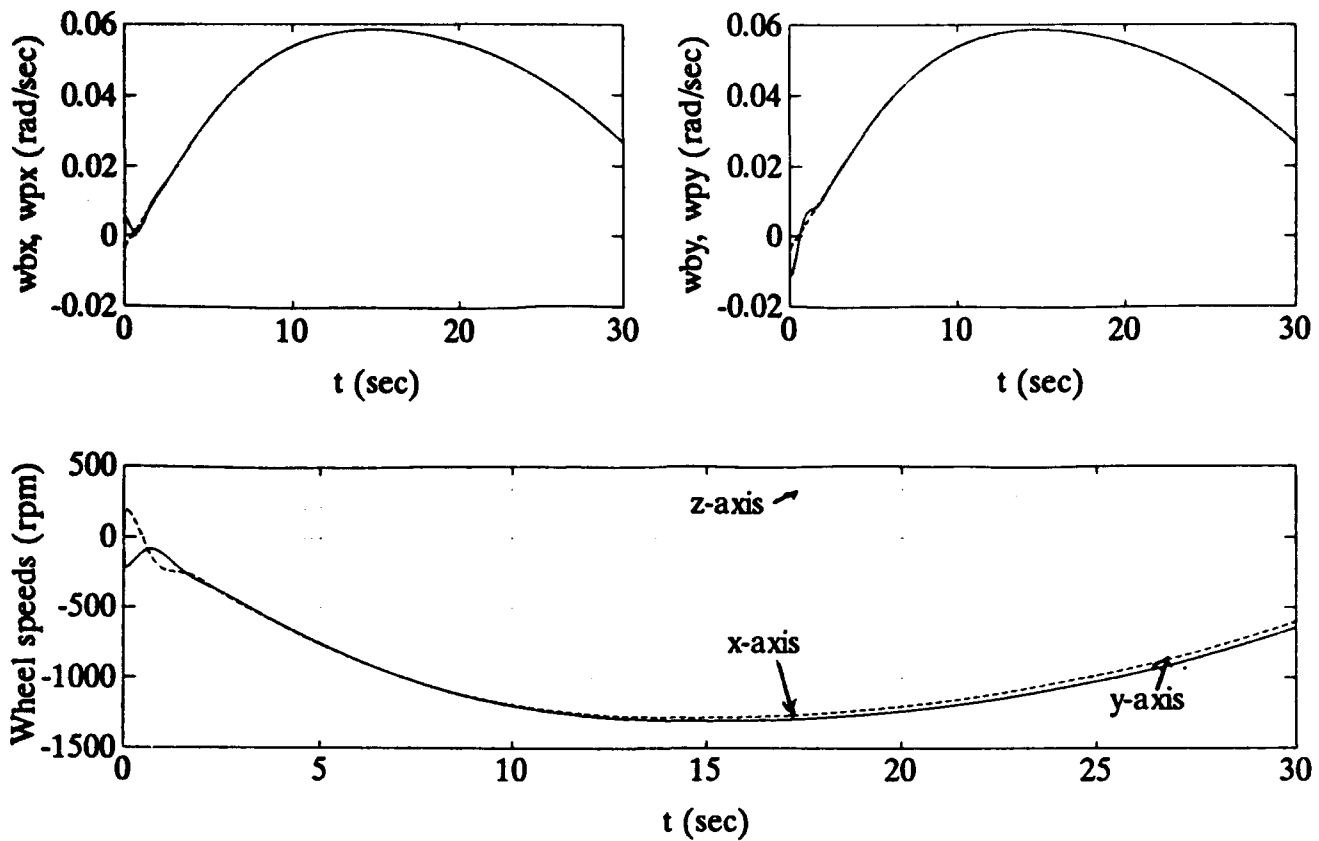
Figure 5-4: Case 1 Results Using Linear Spacecraft Controller with Inertia Tensor Uncertainty

tion with the spacecraft nonlinear controller shows a performance advantage in controlling the angular displacement and also in controlling off-axis torques and wheel speeds.

5.3 Measurement Noise Effects

The simulations to this point have been based on perfect knowledge of sensor data. The whole design approach is deterministic and does not directly address measurement uncertainty. The two critical sensors are the rate gyro commands and the angular displacement sensors. This section addresses a simple model for noise which was simulated using Case 1.

The architecture using the stable platform is based on the assumption that the ISPRU platform responds perfectly to the low bandwidth rate commands in the x and y axes. The commands to the platform are input externally to an already closed loop system which is designed to maintain the gyroscope gimbal orientations stable with respect to inertial space; in
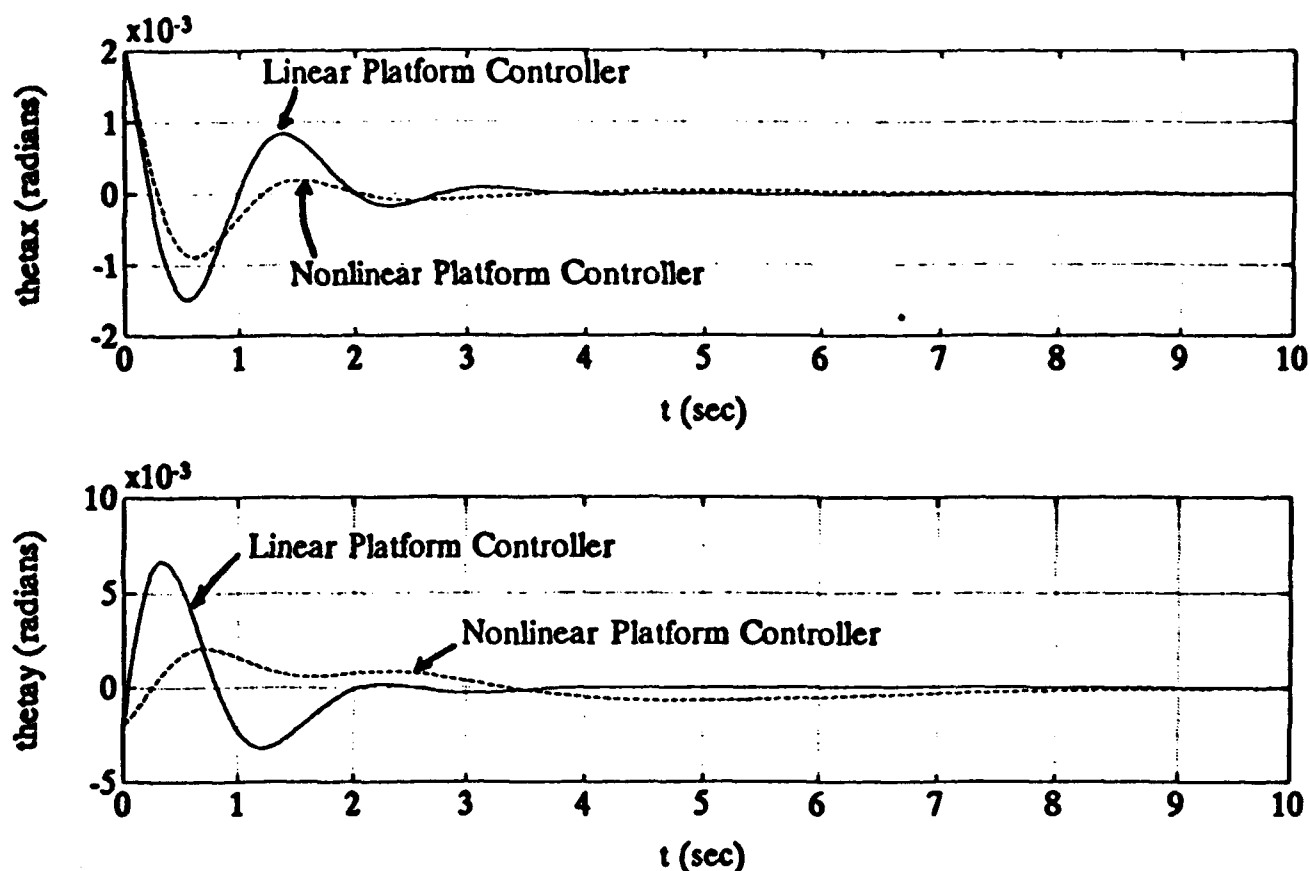
Figure 5-5: Case 2 Angular Displacements with Inertia Tensor Uncertainty

this sense the platform is commanded in an open loop manner. The platform high frequency jitter effect on the spacecraft is minimized by superior gyro performance and the low bandwidth controllers for the platform and spacecraft. However, even the best gyros will drift over time and it is necessary to use external measurements (such as earth, star or sun sensor measurements) to calibrate the gyros. All of the measurement data is filtered (Kalman filter) throughout the orbit to determine an estimate for the gyro drift and angular rates which are then integrated to determine the orientation of the IPSRU platform with respect to inertial space (the direction cosine matrix computer). This filter attempts to compensate for the based on an extremely accurate model based on extensive gyro test data for the model and external attitude references for on-line calibration [20]. Even the best filter will have a residual error which is essentially a low rate drift in the estimation of the angular rate. As a result, "sensor" noise in the context of the IPSRU platform control used here manifests itself as noise in the direction cosine

matrix. The noise simulation was based on the parameters of the expected drift of this rate, and is more accurately described as an error analysis based on inaccurate rate estimation as compared to the direction cosine matrix elements. The simulation of this effect is accomplished by generating a random vector whose parameters match the expected error in the angular rate estimation for the platform, which is then treated as additive uncertainty to the IPSRU commands ω_{P_x} and ω_{P_y}. The plots are not shown, but the result is a direction cosine component error which is proportional to the magnitude of the commanded rates. The persistence, or constant bias, seemed to be the critical factor, as opposed to the variations around the bias which are essentially filtered out by the low bandwidth control, as would be expected. This error needs additional analysis; one method would be to propagate the kinematics of an angular displacement of the direction cosine matrix.

The sensor noise model for the angular displacement sensor was calculated from the manufacturer's specification for the sensor. The noise is considered zero mean with variation of approximately 3e-9 rad for the frequency range of the angular displacement regulator, and simulations indicated no apparent effects of this noise, either in the angular displacement itself or in the effects on the coordinate transformations for the direction cosine matrix C_P^B.

5.4   Spacecraft Control Simulation Results

The control architecture used in the simulations appears quite feasible in the context of the idealizations and the limited simulations of uncertainties due to inertia tensor uncertainties and measurement noise. Several issues which affect the controller performance were raised in the simulation and design of the controllers:

1. The nonlinear controller for the IPSRU platform results in lower peak wheel speeds than the linear controller when the same spacecraft controller is used for each case.

2. The nonlinear controller for the spacecraft provides significant improvement in transient performance compared to a linear spacecraft controller when inertia uncertainties are considered.

3. The IPSRU platform control may be essentially treated as a free body provided the angular displacement between the platform and spacecraft remains below the limits of